Article

Cell Reports

Cathepsin G Inhibition by Serpinb1 and Serpinb6 Prevents Programmed Necrosis in Neutrophils and Monocytes and Reduces GSDMD-Driven Inflammation

Graphical Abstract

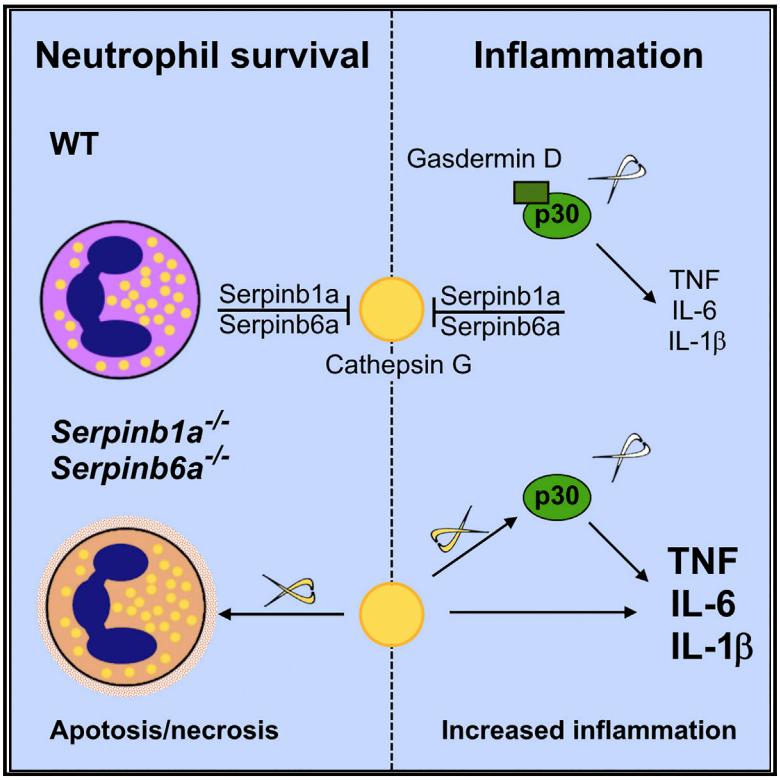

Authors

Sabrina Sofia Burgener, Nathan Georges François Leborgne, Scott J. Snipas, Guy S. Salvesen, Phillip Ian Bird, Charaf Benarafa

Correspondence

charaf.benarafa@vetsuisse.unibe.ch

In Brief

Burgener et al. show that cytosolic protease inhibitors Serpinb1a and Serpinb6a inhibit the granule serine protease cathepsin G to prevent neutrophil and monocyte death and cytokine release upon LPS challenge. Mechanistically, activation of gasdermin D by cathepsin G is required for inflammation but not for neutrophil death.

Highlights

- Serpinb1a and Serpinb6a prevent cathepsin G-dependent neutrophil death
- Cathepsin G cleaves gasdermin D at Leu^{274} to generate a p30 fragment
- Serpin deficiency leads to high inflammation via cathepsin G and gasdermin D
- Gasdermin D does not regulate neutrophil death in serpin deficiency

Burgener et al., 2019, Cell Reports *27*, 3646–3656
June 18, 2019
https://doi.org/10.1016/j.celrep.2019.05.065

CellPress

OPEN ACCESS
CellPress

Cell Reports
Article

Cathepsin G Inhibition by Serpinb1 and Serpinb6 Prevents Programmed Necrosis in Neutrophils and Monocytes and Reduces GSDMD-Driven Inflammation

Sabrina Sofia Burgener,[1,2,3] Nathan Georges François Leborgne,[1,2,3] Scott J. Snipas,[4] Guy S. Salvesen,[4] Phillip Ian Bird,[5] and Charaf Benarafa[1,2,6,*]

[1]Institute of Virology and Immunology, 3147 Mittelhäusern, Switzerland
[2]Department of Infectious Diseases and Pathobiology, Vetsuisse Faculty, University of Bern, 3012 Bern, Switzerland
[3]Graduate School for Cellular and Biomedical Sciences, University of Bern, 3012 Bern, Switzerland
[4]Sanford Burnham Prebys Medical Discovery Institute, La Jolla, CA 92037, USA
[5]Department of Biochemistry and Molecular Biology, Biomedicine Discovery Institute, Monash University, Melbourne, VIC 3800, Australia
[6]Lead Contact
*Correspondence: charaf.benarafa@vetsuisse.unibe.ch
https://doi.org/10.1016/j.celrep.2019.05.065

SUMMARY

Neutrophil granule serine proteases contribute to immune responses through cleavage of microbial toxins and structural proteins. They induce tissue damage and modulate inflammation if levels exceed their inhibitors. Here, we show that the intracellular protease inhibitors Serpinb1a and Serpinb6a contribute to monocyte and neutrophil survival in steady-state and inflammatory settings by inhibiting cathepsin G (CatG). Importantly, we found that CatG efficiently cleaved gasdermin D (GSDMD) to generate the signature N-terminal domain GSDMD-p30 known to induce pyroptosis. Yet GSDMD deletion did not rescue neutrophil survival in *Sb1a.Sb6a*$^{-/-}$ mice. Furthermore, *Sb1a.Sb6a*$^{-/-}$ mice released high levels of pro-inflammatory cytokines upon endotoxin challenge *in vivo* in a CatG-dependent manner. Canonical inflammasome activation in *Sb1a.Sb6a*$^{-/-}$ macrophages showed increased IL-1β release that was dependent on CatG and GSDMD. Together, our findings demonstrate that cytosolic serpins expressed in myeloid cells prevent cell death and regulate inflammatory responses by inhibiting CatG and alternative activation of GSDMD.

INTRODUCTION

Regulated forms of cell death are essential for the development of multicellular organisms and for their immune responses. Apoptosis, the most studied form of regulated cell death (RCD), is triggered by intrinsic or extrinsic cues transmitted to signaling routes converging on the proteolytic activation of executioner caspases. These apoptotic caspases cleave multiple protein targets in the nucleus, the cytoplasm, and the cytoskeleton but do not directly compromise the integrity of the plasma membrane (Taylor et al., 2008). Apoptosis therefore proceeds slowly and without alarming neighboring cells; indeed, the removal of apoptotic bodies by phagocytes induces the release of anti-inflammatory signals (Ravichandran, 2011). Until recently, RCD was synonymous with apoptosis, but it is now recognized that RCD may also involve necrosis resulting from distinct molecular pathways that have been principally defined as necroptosis and pyroptosis (Bliss-Moreau et al., 2017; Wallach et al., 2016). Such pathways may have evolved to trigger inflammation in response to potentially concealed infections and cytosolic microbes (Jorgensen et al., 2017; Miao et al., 2010). Necroptosis occurs in many cell types and can be triggered by tumor necrosis factor-α (TNF-α) as well as other stimuli converging on receptor-interacting protein kinase-3 (RIPK3) (Cho et al., 2009; He et al., 2009; Zhang et al., 2009), which phosphorylates the pseudo-kinase mixed-lineage kinase-like protein (MLKL). Phosphorylated MLKL oligomerizes, leading to cell death (Murphy et al., 2013). Pyroptosis has been principally described in monocytes and macrophages and is elicited by inflammatory caspases, caspase-1/4/5/11 (Miao et al., 2010). This form of RCD is molecularly defined by the specific, limited cleavage of gasdermin D (GSDMD) to release its N-terminal domain GSDMD-p30 (He et al., 2015; Kayagaki et al., 2015; Shi et al., 2015). GSDMD-p30 assembles to form pores at the plasma membrane leading to cell lysis (Aglietti et al., 2016; Ding et al., 2016; Liu et al., 2016).

Neutrophils are major effectors of the immune response to infection and drive inflammatory reactions. Neutrophil serine proteases (NSPs) (e.g., neutrophil elastase [NE], cathepsin G [CatG], proteinase-3 [PR3], and NSP4) contribute to these functions in multiple ways. NSPs are found in specialized secretory lysosomes that fuse with phagosomes or are released into the extracellular milieu upon degranulation. NSPs have antimicrobial functions through defined proteolysis of microbial toxins and structural proteins (Belaaouaj et al., 2000; Tkalcevic et al., 2000; Weinrauch et al., 2002). Importantly, NSPs promote inflammation through cleavage-mediated activation or inhibition of cytokines, chemokines, opsonins, and receptors (Clancy et al., 2018; Henry et al., 2016; Kessenbrock et al., 2008; Lefrançais et al., 2012; Padrines et al., 1994; Raptis et al., 2005). NSPs have been associated with neutrophil death, but the mechanisms are not fully elucidated and appear different for each NSP (Benarafa and Simon, 2017). Most notably, heterozygous

mutations in the gene for NE, *ELANE*, are the most common cause of severe congenital neutropenia and the only known cause of cyclic neutropenia (Makaryan et al., 2015). NE is expressed at high levels at the promyelocyte stage and mutant proteins induce cell death and an apparent maturation block at the promyelocyte stage. How the various NE mutants induce cell death is not defined, but it may be due to the unfolded protein response or to mislocalized mutant NE because NE proteolytic activity is not required (Tidwell et al., 2014). By contrast, CatG and PR3 can directly activate apoptotic pro-caspase-7 and pro-caspase-3, respectively (Loison et al., 2014; Zhou and Salvesen, 1997). NSPs are also expressed in a subset of monocytes (Kargi et al., 1990). Recent evidence suggests that NSP-expressing monocytes derive from a neutrophil-like common ancestor (Yanez et al., 2017), but the function of NSPs in monocyte homeostasis is unknown.

Secreted endogenous inhibitors regulate the activity of NSPs in plasma (e.g., α1-antitrypsin) and mucosal surfaces (e.g., secretory leukocyte protease inhibitor [SLPI]). Inhibitors of the clade B serpin family are cytosolic and expressed in monocytes and neutrophils (Remold-O'Donnell et al., 1989; Scott et al., 1999). Among the latter, Serpinb1 is found at high levels in the cytosol of neutrophils and monocytes and inhibits all NSPs except NSP4 (Benarafa et al., 2011; Cooley et al., 2001; Perera et al., 2012). Mice deficient in the mouse ortholog *Serpinb1a* (*Sb1a*$^{-/-}$) have reduced neutrophil numbers, show increased mortality, and produce high levels of inflammatory cytokines upon lung infection (Benarafa et al., 2007, 2011; Gong et al., 2011). Serpinb6 is a related clade B serpin, also expressed in monocytes and neutrophils, which inhibits CatG but not NE or PR3 (Scott et al., 1999). Notably, deficiency in the mouse ortholog, *Serpinb6a* (*Sb6a*$^{-/-}$), was not associated with defects in leukocyte numbers, possibly because Serpinb1a levels are higher in these animals (Scarff et al., 2004). In this study, we first investigated the effects of combined deficiency of *Sb1a* and *Sb6a* (*Sb1a.Sb6a*$^{-/-}$) on leukocyte homeostasis and the effect on RCD pathways of monocytes and neutrophils *in vitro*. We discovered that the two serpins collaborate to protect myeloid cells through blockade of cell-specific, CatG-dependent RCD. We found that CatG efficiently cleaves GSDMD to generate GSDMD-p30, but deletion of GSDMD did not rescue CatG-mediated neutrophil death *in vivo* and *in vitro*. In contrast, we demonstrated that *Sb1a.Sb6a*$^{-/-}$ mice released more IL-1β, TNF-α, and IL-6 in a CatG- and GSDMD-dependent manner in *in vivo* models of inflammation and following classical inflammasome activation in macrophages *in vitro*.

RESULTS

Serpinb1a and Serpinb6a Are Survival Factors for Neutrophils *In Vivo*

To address the function of Sb1a and Sb6a in myeloid cell homeostasis, we analyzed the leukocyte subsets from single- and double-deficient 6-week-old mice in steady state. *Sb1a.Sb6a*$^{-/-}$ mice showed a severe reduction in absolute numbers and proportion of neutrophils in the bone marrow (Figures 1A, S1A, and S1B). The neutropenia of *Sb1a.Sb6a*$^{-/-}$ mice was more severe than that observed in *Sb1a*$^{-/-}$ mice; and *Sb6a*$^{-/-}$ mice had normal proportions and numbers of neutrophils (Figure S1B; Benarafa et al., 2011; Scarff et al., 2004). Neutrophil counts in blood were significantly reduced only in *Sb1a.Sb6a*$^{-/-}$ mice compared to wild-type (WT) mice (Figure S1C). Sb1a and Sb6a are both inhibitors of CatG (Benarafa et al., 2002; Scott et al., 1999), and CatG deletion rescues the neutropenia of *Sb1a*$^{-/-}$ mice (Baumann et al., 2013). Thus, we generated mice lacking both serpins and CatG and found that deletion of CatG was indeed sufficient to restore normal neutrophil numbers in bone marrow and blood in steady state (Figures 1A and S1C).

Neutrophils are rapidly mobilized from the bone marrow in response to infection and have a high phagocytic capacity. To evaluate the relevance of the neutropenia of *Sb1a.Sb6a*$^{-/-}$ mice on neutrophil recruitment and efficient clearance of fungal particles, we injected opsonized zymosan intraperitoneally. We observed a reduced number of peritoneal neutrophils in *Sb1a.Sb6a*$^{-/-}$ mice 4 h after zymosan injection (Figure 1B). Furthermore, the removal of zymosan was impaired as extracellular particles were still visible in cytospins of peritoneal washes of *Sb1a.Sb6a*$^{-/-}$ mice, there were higher numbers of neutrophils containing yeast particles, and more zymosan per phagocyte was observed compared to WT mice (Figure 1C). Defective neutrophil recruitment and impaired clearance of zymosan particles were fully rescued in *CatG.Sb1a.Sb6a*$^{-/-}$ mice (Figures 1B and 1C). Thus, control of CatG by Sb1a and Sb6a is crucial to maintain neutrophil survival in steady state and to support efficient innate immune responses.

Apoptotic and Necrotic Pathways in Neutrophils Are Accelerated by CatG

Loss of granule membrane integrity can result in the cytosolic release of proteases, which trigger RCD pathways unless opposed by endogenous protease inhibitors (Baumann et al., 2013; Bird et al., 1998, 2014; Luke et al., 2007). Cell death of bone marrow neutrophils was therefore evaluated *in vitro* following treatment with the lysosomotropic compound L-leucyl-L-leucine-methyl-ester (LLME), which is assembled in membranolytic metabolites by the transferase activity of the cysteine protease dipeptidyl-peptidase I (DPPI) to release granule contents into the cytosol (Thiele and Lipsky, 1990). Reflecting the *in vivo* phenotype, *Sb1a.Sb6a*$^{-/-}$ neutrophils were highly sensitive to LLME-induced cell death (Figures 2A and S2A). *Sb1a.Sb6a*$^{-/-}$ neutrophils died significantly faster than *Sb1a*$^{-/-}$ neutrophils (1 h) after LLME treatment, and few neutrophils remained alive after 2 and 4 h in both genotypes. *Sb6a*$^{-/-}$ neutrophils showed an intermediate phenotype between *Sb1a*$^{-/-}$ and WT neutrophils (Figure S2B). Live-cell microscopy recordings of bone marrow cells treated with LLME indicated that *Sb1a*$^{-/-}$ and *Sb1a.Sb6a*$^{-/-}$ cells initiate an accelerated death process measurable 30 min after LLME treatment (Figures S2C and S2D). LLME-induced cell death was not significantly altered by treatment with the broad caspase inhibitor Q-VD-OPh alone or in combination with the RIPK1 inhibitor necrostatin-1 (Figure S2B). In contrast, LLME-induced cell death was fully prevented in *CatG.Sb1a.Sb6a*$^{-/-}$ neutrophils, where *CatG.Sb1a.Sb6a*$^{-/-}$ neutrophils exhibited significantly improved survival compared to *Sb1a.Sb6a*$^{-/-}$ (Figures 2A and S2E).

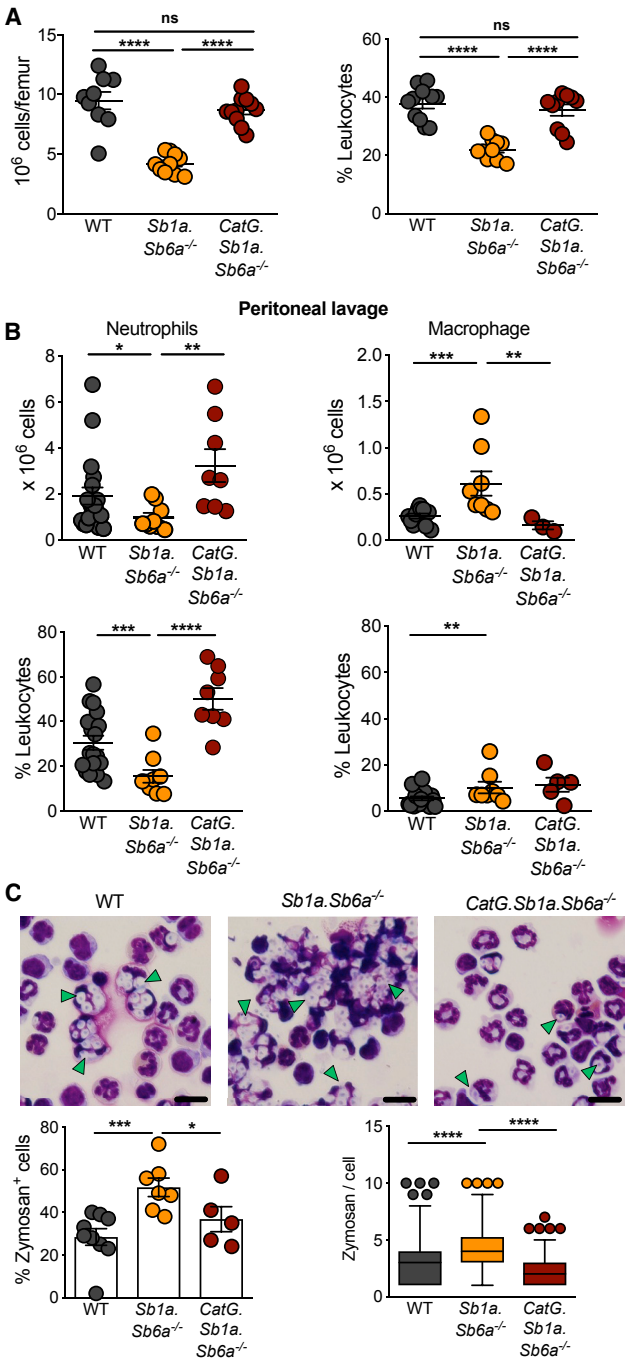

Figure 1. *Sb1a.Sb6a*$^{-/-}$ Mice Present a CatG-Dependent Neutropenia in Steady State and Inflammation

(A) Analysis of bone marrow neutrophils of 6-week-old female mice; n = 10–11/genotype.

(B) Percentage and absolute counts of neutrophils and macrophages in peritoneal lavage fluid 4 h after injection of 0.5 mg of zymosan/mouse; n = 8–16/genotype of 6-week-old female and male mice.

(A and B) Scatterplots show data for individual mice from 4 independent experiments; horizontal lines indicate mean ± SEM. Data were analyzed by Mann-Whitney test (****p < 0.0001; ***p < 0.001; **p < 0.01; *p < 0.05; ns, p > 0.05).

Neutrophils have a limited life span *in vitro* due to spontaneous apoptosis mediated principally by the intrinsic mitochondrial apoptotic pathway culminating with activation of apoptotic caspase-3 and -7 (Geering and Simon, 2011). Apoptotic neutrophils then rapidly proceed to secondary necrosis. Cultured *Sb1a.Sb6a*$^{-/-}$ neutrophils showed increased necrosis in the presence of the caspase inhibitor (Figures 2B and S3A). This defect was dependent on CatG since *CatG.Sb1a.Sb6a*$^{-/-}$ neutrophil spontaneous death *in vitro* was indistinguishable from that of WT neutrophils. Percentages of apoptotic cells, measured by annexin V staining, were not significantly different between cells of different genotypes (Figures 2B and S3A).

Neutrophils are sensitive to death receptor stimulation, which leads to apoptosis or necroptosis depending on caspase-8 activity and X-linked inhibitor of apoptosis (XIAP) (Wang et al., 2018; Wicki et al., 2016). Neutrophils were stimulated with TNF-α for 24 and 48 h leading to a massive induction of cell death that was indistinguishable between genotypes. Caspase inhibition with Q-VD-OPh considerably reduced TNF-induced neutrophil death in all genotypes. Yet *Sb1a.Sb6a*$^{-/-}$ neutrophils showed increased necrosis and reduced apoptosis in a CatG-dependent manner (Figures 2C and S3B). Necroptosis induced by TNF-α depends on the interaction of RIPK1 and RIPK3, which is allowed by RIPK1 autophosphorylation (Cho et al., 2009). Inhibition of RIPK1 with necrostatin-1 in presence of Q-VD-OPh reduced neutrophil necrosis in all genotypes but did not abrogate the increased necrosis observed in *Sb1a.Sb6a*$^{-/-}$ neutrophils (Figures 2C and S3B).

Reactive oxygen species (ROS) produced by the NADPH-oxidase contribute to neutrophil death in inflammatory conditions (von Gunten et al., 2005). To explore the role of ROS, we evaluated leukocyte subsets of mice lacking the critical p47phox subunit of the NADPH oxidase (Huang et al., 2000). We found that both *Ncf1.Sb1a*$^{-/-}$ and *Sb1a*$^{-/-}$ mice presented similarly reduced neutrophil numbers in the bone marrow compared to WT and *Ncf1.*$^{-/-}$ mice in steady state (Figures S3C and S3D). Granzymes and caspases can induce ROS-mediated cell death by cleaving mitochondrial complex I subunit NDUFS1 (Martinvalet et al., 2008). Scavenging of mitochondrial ROS with MitoQ did not significantly alter LLME-induced and TNF-induced neutrophil death (Figures S3E and S3F). We found that CatG did not cleave the respiratory chain components NDUFS1 and NDUFS3 in *Sb1a.Sb6a*$^{-/-}$ neutrophils (Figure S3G). Overall, these data indicate that Sb1a and Sb6a inhibit CatG-mediated apoptotic and necrotic death induced by multiple stimuli such as survival factor withdrawal, death receptor stimulation, and loss of granule integrity. Yet neutrophil death was partly

(C) Representative cytospins of peritoneal cells; quantification of zymosan-containing cells and of number of zymosan particles per neutrophil. Data are from male and female mice; n = 5–9/genotype from 4 independent experiments and analyzed by one-way ANOVA (****p < 0.0001; ***p < 0.001). Left panel: percentage of zymosan-positive cells for individual mice; bars indicate mean ± SEM. Right panel: numbers of zymosan particles per neutrophil (40 neutrophils/mouse from 5–9 mice/genotype) for all mice per genotype; data are shown as box and whiskers (****p < 0.0001). Scale bars: 15 μm.

See also Figure S1 and Tables S1 and S2.

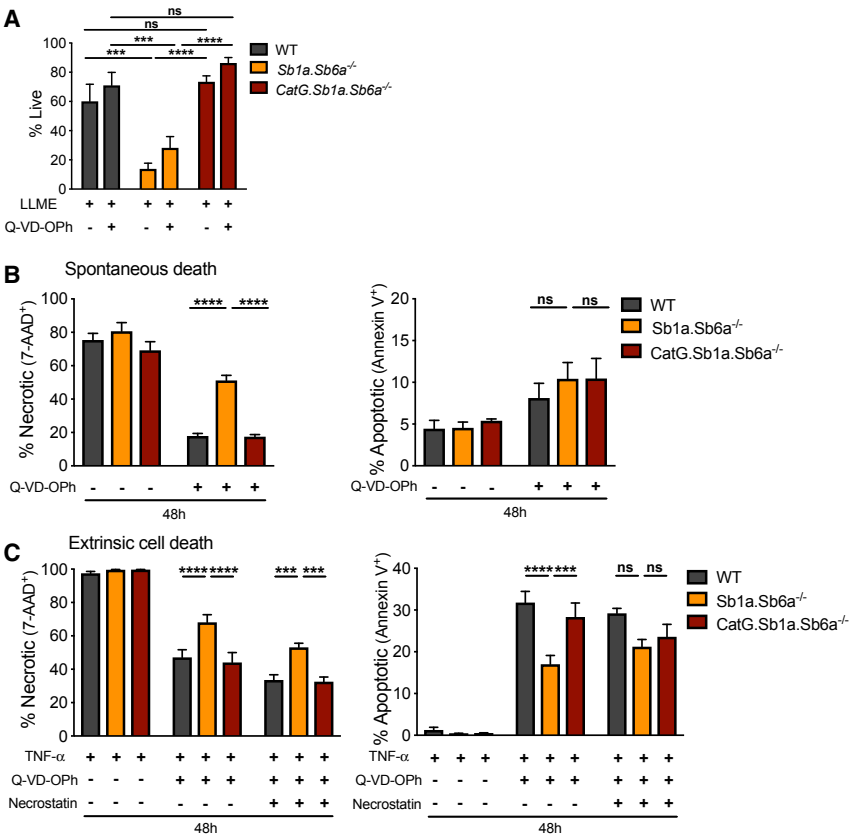

Figure 2. CatG-Dependent Necrosis Is Executed following Induction of Multiple RCD Pathways in *Sb1a.Sb6a*$^{-/-}$ Neutrophils

(A) Survival of neutrophils treated with 100 μM LLME in the presence or absence of 50 μM Q-VD-OPh for 4 h.

(B) Spontaneous apoptosis and secondary necrosis of neutrophils cultured *in vitro* with or without 50 μM Q-VD-OPh.

(C) Neutrophil survival following stimulation with TNF-α (100 ng/mL) and actinomycin D (200 ng/mL) with or without 50 μM Q-VD-OPh and 20 μM necrostatin-1 over 48 h. Viability of neutrophils was assessed by flow cytometry using Annexin V-APC and 7-AAD. Cells were from 6- to 12-week-old female and male mice. Data are shown as mean ± SEM of 4–8 independent experiments and were analyzed by two-way ANOVA. (****$p < 0.0001$; ***$p < 0.001$; ns, $p > 0.05$.) See also Figures S1–S4.

blocked by caspase inhibition and was independent of RIPK1 and ROS.

Compensatory Effects of Sb1a and Sb6a in Monocyte Survival

Beyond neutrophils, *Sb1a.Sb6a*$^{-/-}$ mice presented significantly reduced monocyte numbers and percentage in bone marrow (Figures S1A and S4A). The monocyte defect was largely resolved in the bone marrow of *CatG.Sb1a.Sb6a*$^{-/-}$ mice, which showed monocyte numbers and percentage similar to WT and significantly higher percentage than *Sb1a.Sb6a*$^{-/-}$ mice. *Sb1a*$^{-/-}$ and *Sb6a*$^{-/-}$ single-knockout mice had normal monocyte numbers and percentage in bone marrow, as previously reported (Benarafa, 2011; Scarff et al., 2004) (Figure S4A). Differences in blood monocytes were variable and showed a subtle downward trend for *Sb6a*$^{-/-}$ and *Sb1a.Sb6a*$^{-/-}$ mice (Figure S4B). No difference between the genotypes was observed in other major blood leukocyte subsets and erythrocytes (Tables S1 and S2). Monocytes were generally less sensitive to LLME than neutrophils, and only *Sb1a.Sb6a*$^{-/-}$ monocytes showed a significant increase in necrotic cell death following LLME treatment compared to WT (Figures S4C and S4D). Cell death in *Sb1a*$^{-/-}$ and *Sb6a*$^{-/-}$ monocytes treated with LLME were at intermediate levels between WT and *Sb1a.Sb6a*$^{-/-}$ (Figure S4D). In *Sb1a.Sb6a*$^{-/-}$ mice, deletion of CatG only partly corrected the accelerated monocyte death after LLME treatment (Figure S4E). As in neutrophils, the *in vivo* and *in vitro* findings suggest that Sb1a and Sb6a additively, although modestly, contribute to monocyte survival.

CatG Directly Cleaves GSDMD into a Stable N-Terminal Domain GSDMD-p30

Because CatG induces a regulated form of necrosis with fast kinetics, we hypothesized that CatG might process GSDMD to induce cell lysis. We indeed found that purified human CatG cleaved both human and mouse GSDMD to form a stable characteristic GSMD-p30 fragment virtually indistinguishable from that generated by recombinant mouse caspase-11 (Figures 3A, 3B, S5A, and S5B). Under the conditions used, purified human NE and PR3 failed to produce a stable GSDMD-p30 fragment at low nanomolar concentrations and had a largely degrading activity on human and mouse GSDMD at higher concentrations (Figures 3C, 3D, S5C, and S5D). Pretreatment of the proteases with the caspase inhibitor Q-VD-OPh blocked the cleavage of GSDMD by caspase-11 but not by CatG, ruling out indirect activation of caspases in THP-1 and transfected HEK cell lysates (Figure S5A). Conversely, CatG inhibitor I (CatG-Inh) had no effect on caspase-11 activity, while effectively inhibiting CatG (Figures S5A–S5D). We found that cleavage of mouse GSDMD by high concentrations of NE was inhibited by CatG-Inh, suggesting that the observed cleavage may not be caused by NE but by residual CatG activity in the purified preparation of NE from human sputum (Figure S5C).

Purified recombinant mouse GSDMD with a C-terminal His-tag (rGSDMD) and active site titrated CatG were used to determine the second order rate constant for CatG cleavage of GSDMD (Figure S5E). The k_{cat}/K_M value was 1.09×10^6 $M^{-1} \cdot s^{-1}$, which is one or two order of magnitude greater than what we previously reported for caspase-1 ($<10^5$ $M^{-1} \cdot s^{-1}$) and caspase-11 ($<10^4$ $M^{-1} \cdot s^{-1}$), respectively (Gonzalez Ramirez et al., 2018). The p20 C-terminal fragment generated by CatG was excised and subjected to Edman degradation to reveal that CatG cleaved

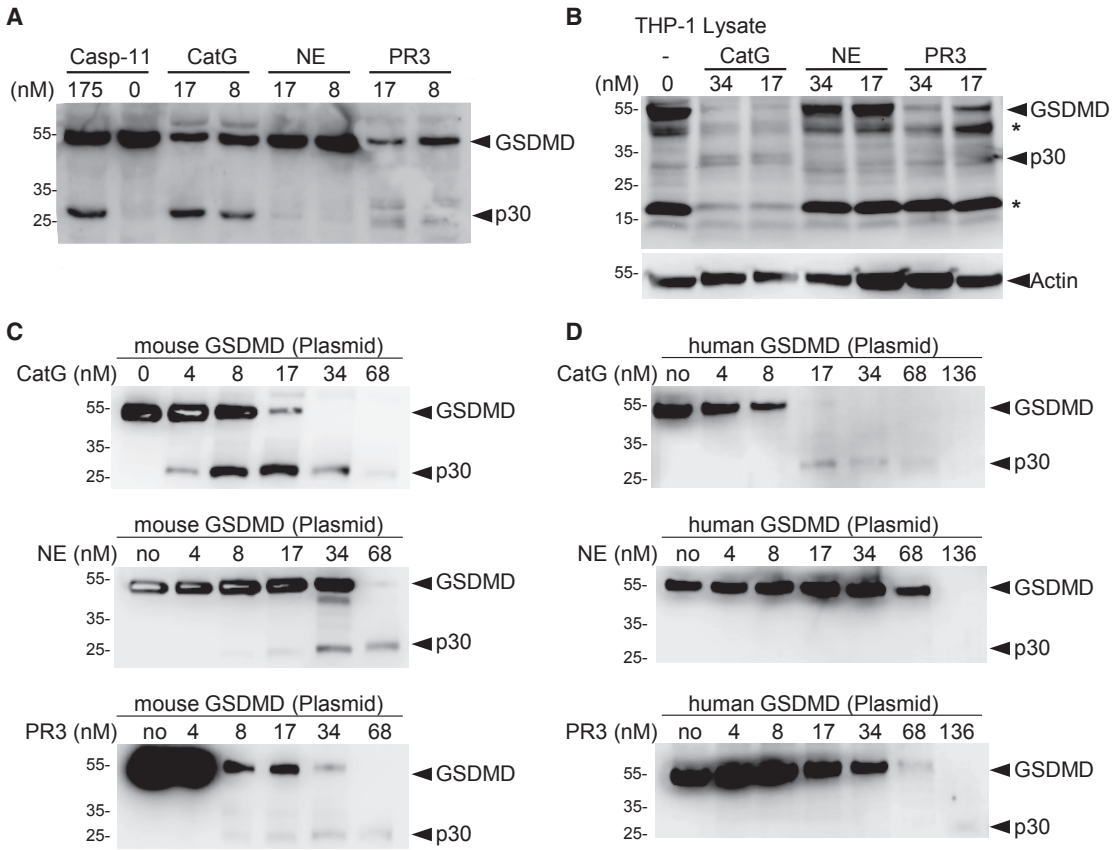

Figure 3. CatG Cleaves GSDMD to Generate GSDMD-p30 N-Terminal Fragment

Immunoblots of (A) HEK cells, transfected with mouse Flag-GSDMD plasmid; (B) THP-1 lysates; (C) HEK cells, transfected with mouse Flag-GSDMD plasmid; and (D) HEK cells, transfected with human Flag-GSDMD plasmid. Cells were lysed without protease inhibitors, incubated (12.5–25 μg total proteins) with indicated concentrations of proteases (nanomolar) for 1 h at 37°C and were resolved on SDS-PAGE and immunoblotted for GSDMD (B) or Flag (A, C, and D). See also Figure S5.

GSDMD at Leu-274 (Figures S5E and S5F). Substitution of Leu-274 for Ala (L274A) or for Gly (L274G) substantially reduced the cleavage of GSDMD by CatG (Figure S5G). Incomplete abrogation of CatG cleavage of the L274 mutants suggests that alternative, less preferred, cleavage sites for CatG may exist in the linker region between the N- and C-terminal regions when high protease concentrations are used (Figure S5F). Together, these findings demonstrate that GSDMD is a preferred substrate of CatG, which cleaves GSDMD only two residues upstream of the caspase cleavage site at Asp-276 (Kayagaki et al., 2015; Shi et al., 2015).

Sb1a.Sb6a$^{-/-}$ Neutropenia Is Not Due to Pyroptosis Mediated by GSDMD

We then ruled out a role for pyroptotic caspases in the steady-state neutropenia due to Sb1a deficiency. Deletion of both mouse inflammatory caspases (*Casp1* and *Casp11*) did not rescue the bone marrow neutropenia in *Casp1/11.Sb1a*$^{-/-}$ mice (Figures S6A and S6B). Furthermore, we observed no difference in cell death kinetics after granule permeabilization of *Casp1/11.Sb1a*$^{-/-}$ neutrophils compared to *Sb1a*$^{-/-}$ neutrophils treated with LLME (Figure S6C). To address whether Gsdmd is required for neutrophil death *in vivo*, we generated *Gsdmd* knockout mice by CRISPR/Cas9 targeting in *Sb1a.Sb6a*$^{-/-}$ zygotes. Five mutant alleles were identified, and each was bred to homozygosity (Figure S7). We found that *Gsdmd.Sb1a.Sb6a*$^{-/-}$ had reduced neutrophils in the bone marrow similarly as *Sb1a.Sb6a*$^{-/-}$ mice, while *Gsdmd*$^{-/-}$ neutrophil numbers were the same as in WT mice in steady state (Figure 4A). Furthermore, granule permeabilization with LLME induced identical kinetics of necrosis in *Gsdmd.Sb1a.Sb6a*$^{-/-}$ as in *Sb1a.Sb6a*$^{-/-}$ neutrophils (Figures 4B and S8A). Likewise, spontaneous apoptosis was not altered in neutrophils lacking *Gsdmd* in WT or *Sb1a.Sb6a*$^{-/-}$ backgrounds (Figures 4C and S8B). We also found that TNF-mediated death pathways were consistently increased in *Gsdmd.Sb1a.Sb6a*$^{-/-}$ (as in *Sb1a.Sb6a*$^{-/-}$) compared to *Gsdmd*$^{-/-}$ and WT neutrophils (Figures 4D and S8C). Deletion of *Gsdmd* appears to reduce monocyte numbers in the bone marrow compared to WT mice, but no further decrease in monocyte numbers and percentage was observed in *Gsdmd.Sb1a.Sb6a*$^{-/-}$ compared to *Sb1a.Sb6a*$^{-/-}$ bone marrow (Figure S8D). Moreover, LLME-induced death was similarly enhanced in *Gsdmd.Sb1a.Sb6a*$^{-/-}$ and *Sb1a.Sb6a*$^{-/-}$ monocytes, and no difference was observed between WT and *Gsdmd*$^{-/-}$ monocytes in this assay (Figure S8E).

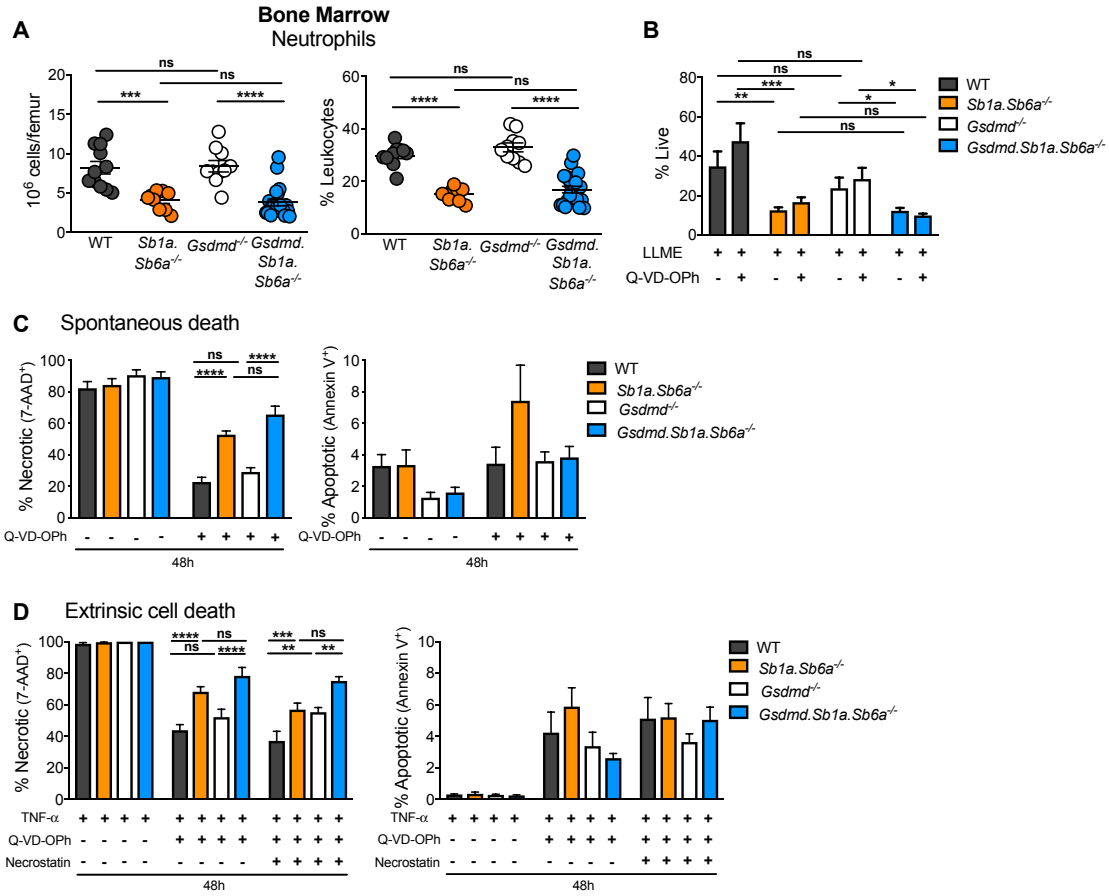

Figure 4. GSDMD Does Not Mediate Neutrophil Death in *Sb1a.Sb6a*$^{-/-}$ Mice

(A) Leukocyte subset analysis of bone marrow neutrophils of 6-week-old male and female mice; n = 9–16/genotype from 6 independent experiments. Scatterplots show data for individual mice; horizontal lines indicate mean ± SEM. Data were analyzed by Mann-Whitney test (****p < 0.0001; ***p < 0.001; ns, p > 0.05).

(B) Survival of neutrophils treated with 100 μM LLME in the presence or absence of 50 μM Q-VD-OPh for 4 h.

(C) Spontaneous apoptosis and secondary necrosis of neutrophils cultured *in vitro* with or without 50 μM Q-VD-OPh.

(D) Neutrophil survival following stimulation with TNF-α (100 ng/mL) and actinomycin D (200 ng/mL) with or without 50 μM Q-VD-OPh and 20 μM necrostatin-1 over 48 h. Viability was assessed by flow cytometry using Annexin V-APC and 7-AAD. Cells were from 6- to 12-week-old female and male mice.

(B –D) Data are shown as mean ± SEM of 3–6 independent experiments and were analyzed by two-way ANOVA (****p < 0.0001; ***p < 0.001; **p < 0.01; *p < 0.05; ns, p > 0.05).

See also Figures S6–S8.

Neutrophil and monocyte percentage in blood of *Gsdmd*$^{-/-}$ and *Gsdmd.Sb1a.Sb6a*$^{-/-}$ were similar to each other and intermediate between WT and *Sb1a.Sb6a*$^{-/-}$ (Figure S8F). Higher absolute counts of neutrophils in blood in *Gsdmd.Sb1a.Sb6a*$^{-/-}$ and *Gsdmd*$^{-/-}$ compared to *Sb1a.Sb6a*$^{-/-}$ mice does not reflect a specific rescue but is rather due to elevated total white blood counts (WBCs) in *Gsdmd*$^{-/-}$ and *Gsdmd.Sb1a.Sb6a*$^{-/-}$ compared to other genotypes (Figure S8F; Table S2). Overall, our findings demonstrate that Gsdmd is dispensable for the death pathways mediated by CatG and regulated by Sb1a and Sb6a *in vivo* and *in vitro*.

Sb1a and Sb6a Regulate Endotoxin-Mediated Inflammation in a CatG- and GSDMD-Dependent Manner

Activation of GSDMD by inflammatory caspases and assembly of GSDMD-p30 at the plasma membrane contribute in part to the release of mature IL-1β and *Gsdmd*$^{-/-}$ mice are largely protected against endotoxemic shock (Kayagaki et al., 2015; Shi et al., 2015). Conversely, we have previously shown that *Sb1a*$^{-/-}$ mice release increased levels of inflammatory cytokines in association with failed clearance of *Pseudomonas aeruginosa* infection (Benarafa et al., 2007). To test the physiological relevance of the cleavage of GSDMD by CatG, we measured the early systemic cytokine response to intraperitoneal injection of a sublethal dose of lipopolysaccharide (LPS). We found that *Sb1a.Sb6a*$^{-/-}$ mice had significantly higher levels of TNF-α at 2 h after injection and increased IL-6 and IL-1 β at 6 h compared to WT mice (Figure 5A). Importantly, increased systemic inflammation was dependent on CatG, as cytokine levels in *CatG.Sb1a.Sb6a*$^{-/-}$ mirrored those of WT mice (Figure 5A). As expected, GSDMD was essential for the detection of IL-1β but, importantly, deletion of GSDMD also reduced TNF-α levels

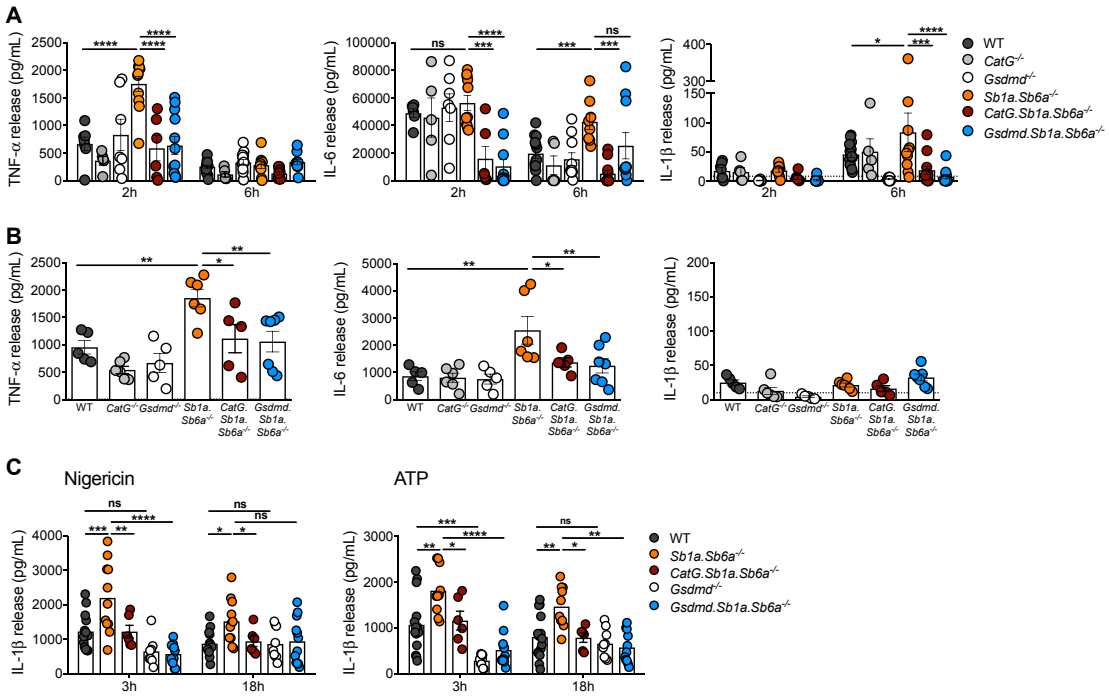

Figure 5. *Sb1a.Sb6a*$^{-/-}$ Mice Exhibit CatG-Dependent Enhanced Pro-inflammatory Responses upon LPS Challenge

(A) Systemic cytokine release in plasma after intraperitoneal injection of LPS. Data are from male and female 6-week-old mice; n = 5–15/genotype from 7 independent experiments and analyzed by two-way ANOVA (****p < 0.0001; ***p < 0.001; *p < 0.05; ns, p > 0.05).

(B) Local cytokine release in BAL after intranasal LPS instillation. Data are from female 6-week-old mice; n = 5–6/genotype from 3 independent experiments and analyzed by one-way ANOVA (**p < 0.01; *p < 0.05).

(C) IL-1β released by BMDMs primed with LPS and stimulated with nigericin and ATP for 3 and 18 h. BMDMs were from 6- to 12-week-old female and male mice. Data are from n = 10–14/genotype from 9 independent experiments and analyzed by one-way ANOVA at each time point (****p < 0.0001; ***p < 0.001; **p < 0.01; *p < 0.05; ns, p > 0.05). All data are shown as mean ± SEM with individual scatterplots.

See also Figure S8.

(2 h) but not IL-6 levels (6 h) in *Gsdmd.Sb1a.Sb6a*$^{-/-}$ mice (Figure 5A). Similarly, in a lung inflammation model induced by intranasal instillation of LPS, *Sb1a.Sb6a*$^{-/-}$ mice showed a significant increase in TNF-α and IL-6 in bronchoalveolar lavage (BAL) 14 h after instillation, and this increase was dependent on both CatG and GSDMD (Figure 5B). At this time point, IL-1β levels in BAL were very low to undetectable in all genotypes.

To evaluate direct effects of the cytosolic serpins on IL-1β release, we finally investigated the effects of canonical inflammasome activation in bone marrow-derived macrophages (BMDMs). We found that IL-1β release by *Sb1a.Sb6a*$^{-/-}$ BMDMs was significantly higher than by WT primed BMDMs stimulated with nigericin or ATP at 3 and 18 h. Furthermore, this effect was again completely dependent on both CatG and GSDMD (Figure 5C). In all conditions, we did not observe any significant difference in cell death (lactate dehydrogenase [LDH] release) between genotypes (Figure S8G). Taken together, our data indicate that Sb1a and Sb6a regulate inflammatory responses through the regulation of CatG and in part through prevention of GSDMD processing in macrophages.

DISCUSSION

Serpinb1 and Serpinb6 are ancient clade B serpin genes and are conserved in all vertebrates (Benarafa and Remold-O'Donnell, 2005; Kaiserman and Bird, 2005). In this study, we found that both mouse orthologs Serpinb1a and Serpinb6a are survival factors of neutrophils and monocytes. In neutrophils, cell death was increased in single serpin knockout mice, and it was significantly more severe in *Sb1a.Sb6a*$^{-/-}$ neutrophils. In monocytes, each serpin compensated for the absence of the other, and reduced survival of monocytes was observed only in double-knockout *Sb1a.Sb6a*$^{-/-}$ mice. Both serpins have very fast inhibitory second order rate constants for CatG, 10^7 mol/L^{-1}•s^{-1} for Serpinb6 and 2 × 10^6 mol/L^{-1}•s^{-1} for Serpinb1 (Cooley et al., 2001; Scott et al., 1999). Since CatG deletion rescues the neutrophil defect of *Sb1a*$^{-/-}$ neutrophils (Baumann et al., 2013), we anticipated and demonstrated that CatG is essential in inducing cell death in *Sb1a.Sb6a*$^{-/-}$ neutrophils in homeostatic conditions *in vivo*. Moreover, granule permeabilization-induced cell death was reduced in *CatG.Sb1a.Sb6a*$^{-/-}$ neutrophils, indicating that the CatG/serpin axis is critical in this neutrophil RCD pathway. In monocytes, CatG deletion also rescued monocyte numbers in mice lacking both serpins.

Increased spontaneous death and TNF-induced death of *Sb1a.S6a*$^{-/-}$ neutrophils *in vitro* also highlighted the contribution of the two serpins in regulating CatG in these RCD pathways. Spontaneous neutrophil apoptosis is largely driven by the intrinsic apoptotic pathway and can be significantly delayed by

sustained expression of anti-apoptotic BCL-2 family proteins such as Mcl-1 and A1 and by apoptotic caspase inhibitors (Akgul et al., 2001). TNF-α induces apoptosis through the activation of RIPK1, p38 MAPK, PI3K, and generation of ROS by the NADPH oxidase triggering caspase-3 cleavage (Geering and Simon, 2011). Caspase inhibition shifts the apoptotic pathway to necroptosis (Wallach et al., 2016). Here, caspase and RIPK1 inhibition improved survival of *Sb1a.S6a*$^{-/-}$ neutrophils in spontaneous and TNF-induced apoptosis, respectively. Yet *Sb1a.S6a*$^{-/-}$ neutrophils showed more necrotic cells at late time points in the presence of these inhibitors. Therefore, while apoptotic caspases and RIPK1-RIPK3-MLKL are the principal drivers of these RCD pathways, CatG significantly and independently contributes to the acceleration of the dying process toward necrosis (cell lysis). Indeed, granule/lysosomal permeabilization is a late event during TNF-induced death or after NLRP3 inflammasome activation; and this process is associated with cleavage of mitochondrial complex 1 proteins and triggered or enhanced by mitochondrial ROS (Heid et al., 2013; Huai et al., 2013; Oberle et al., 2010). In neutrophils, the prime source of ROS is the NADPH oxidase, but we found that deletion of the essential p47phox subunit in *Ncf1.Sb1a*$^{-/-}$ mice did not rescue neutrophil survival *in vivo* and *in vitro*. Furthermore, CatG did not cleave NDUFS1 and NDUFS3, which are essential for the production of ROS by mitochondria and were shown to be proteolytically inactivated by caspases and granzymes to induce apoptosis (Huai et al., 2013; Jacquemin et al., 2015; Martinvalet et al., 2008). The ROS scavenger MitoQ did not alter cell death mediated by LLME and TNF-α in neutrophils *in vitro*, indicating that CatG-mediated RCD can largely proceed independently of ROS.

Live-cell imaging experiments demonstrated that LLME-treated *Sb1a*$^{-/-}$ and *Sb1a.Sb6a*$^{-/-}$ neutrophils proceeded rapidly through necrotic death with cell membrane blebbing, swelling, and rupture suggestive of pyroptosis (Liu and Lieberman, 2017). We found that human CatG directly cleaves human and mouse GSDMD to generate an N-terminal discreet cleavage product. The cleavage site of mouse GSDMD was identified at Leu-274, only two residues upstream of the conserved Asp-276 cleaved by caspase-1/11. This is reminiscent of the activation of caspase-7 by CatG, which is also two residues upstream of the canonical Asp site (Zhou and Salvesen, 1997). Furthermore, the kinetics of cleavage indicates that GSDMD is a preferred substrate of CatG. A recent study reported that excess recombinant NE cleaved GSDMD and that this cleavage of GSDMD induced neutrophil death. They also reported that *Gsdmd*$^{-/-}$ mice were less effective in clearing intraperitoneally injected *E. coli* (Kambara et al., 2018). In our hands, human purified NE did not cleave either human or mouse GSDMD into a stable GSDMD-p30 fragment. CatG inhibitor I inhibited the cleavage of GSDMD with high NE concentrations, indicating the presence of residual CatG in the purified NE preparation. Furthermore, we found that deletion of caspase-1/11 and, more critically, deletion of GSDMD had no effect on the neutropenia of *Sb1a*$^{-/-}$ and *Sb1a.Sb6a*$^{-/-}$ mice. In addition, caspase-1/11 and GSDMD did not directly contribute to cell death induced by granule permeabilization. We previously showed that NE-deficient neutrophils were equally sensitive to granule permeabilization-induced death as WT neutrophils (Baumann et al., 2013). Serpinb1a also inhibits PR3 (Benarafa et al., 2002), which was shown to activate caspase-3 leading spontaneous apoptosis (Loison et al., 2014). We have shown here that PR3 can cleave GSDMD but generates several fragments that are rapidly degraded, and therefore PR3 may disarm GSDMD-dependent pyroptosis. Release of PR3 together with CatG may in part explain why GSDMD is not involved in cell death in neutrophils. Alternatively, similarly to caspase-3, CatG may have multiple target proteins leading to cell death in addition to caspase-7 and GSDMD and only combined disruption of multiple pathways may restore neutrophil survival in the absence of Serpinb1 and Serpinb6.

Importantly, our study revealed that cytosolic serpins regulate inflammatory cytokine responses and this effect was dependent on CatG and GSDMD. We found increased IL-1β release from *Sb1a.Sb6a*$^{-/-}$ activated macrophages and high levels of IL-6 and TNF-α following local and systemic injection of LPS. The increased cytokine levels *in vitro* and *in vivo* were all dependent on CatG and GSDMD, suggesting that the serpins likely regulate release of this inflammatory cytokine in part through inhibition of processing of GSDMD by CatG. Higher levels of IL-1β and danger signals released from necrotic cells in *Sb1a.Sb6a*$^{-/-}$ mice may in turn lead to the sustained production of TNF-α and IL-6. IL-1β is produced in the cytosol as a biologically inactive pro-form that is activated by cleavage of an N-terminal propeptide. NSPs can process several pro-forms of the IL-1 family members, including IL-1β, IL-33, IL-36α, IL-36β, and Il-36γ (Clancy et al., 2018; Hazuda et al., 1990; Henry et al., 2016; Lefrançais et al., 2012; Macleod et al., 2016). While inflammatory caspases have a predominant role in IL-1β processing in activated myeloid cells, NSPs substantially contribute to enhancing the responses *in vivo* (Adkison et al., 2002; Kono et al., 2012). NSPs are thought to contribute to inflammation in part through processing of IL-1 family members after they are released from necrotic cells as unprocessed pro-forms. Indeed, the reported cleavage sites by NSPs on IL-1 cytokines are located N-terminally of the Asp residues cleaved by caspases. Our study suggests an additional pathway where CatG promotes the release of IL-1β cells via GSDMD activation. Thus, more pro-IL-1β may be processed and released by activated myeloid cells when cytosolic serpins are downregulated or overwhelmed by proteases leading to enhanced release via GSDMD processing by CatG. This may explain in part previous observations of increased release of IL-1β in lungs of *Sb1a*$^{-/-}$ mice infected with *Pseudomonas aeruginosa* or influenza A virus (Benarafa et al., 2007; Gong et al., 2011). Whether this process is occurring with other IL-1 family cytokines and in other cells than macrophages is currently under study. As we were resubmitting this revised manuscript, a study reported a non-covalent interaction between C-terminal domain of Serpinb1 and the CARD domain of inflammatory caspases that was proposed to prevent spontaneous caspase activation (Choi et al., 2019). They show that *Sb1a*$^{-/-}$ mice are more susceptible to a lethal dose of LPS and to bacterial infection. These data are in agreement with our current data and our previous studies showing that clearance of *P. aeruginosa* is reduced in *Sb1a*$^{-/-}$ mice. However, we have also shown that clearance of *P. aeruginosa* can be rescued by

increasing neutrophil numbers following enhanced myelopoiesis with granulocyte-colony stimulating factor (G-CSF) treatment (Basilico et al., 2016). In contrast to the recent report by Choi et al. (2019), we did not observe increased spontaneous release of IL-1β when macrophages were incubated with LPS for 5 h in absence of nigericin or ATP (Figure S8H). Thus, without contradicting a potential direct interaction between caspases and Sb1a shown by these authors, our data presented here demonstrate a more conventional and straightforward mechanism dependent on CatG inhibition by Serpinb1a and Serpinb6a leading to inflammation via GSDMD processing.

In summary, our findings indicate that Serpinb1a and Serpinb6a are key survival factors in neutrophils and monocytes. They protect neutrophils from multiple death pathways through inhibition of CatG, which activates both executors of apoptosis and of pyroptosis: caspase-7 and GSDMD, respectively. Yet our data indicate that CatG does not rely exclusively on any of the known RCD pathways. By contrast, GSDMD is a critical target of CatG-mediated death of monocytes in steady state *in vivo* but not after granule permeabilization. Finally, we demonstrate that Serpinb1a and Serpinb6a critically regulate IL-1β release and systemic inflammation by regulating myeloid cell necrosis and an alternative activation of GSDMD.

STAR★METHODS

Detailed methods are provided in the online version of this paper and include the following:

- KEY RESOURCES TABLE
- CONTACT FOR REAGENT AND RESOURCE SHARING
- EXPERIMENTAL MODEL AND SUBJECT DETAILS
  - Mouse husbandry
  - Previously described mouse lines
  - Newly generated mouse lines
  - Mouse cohorts
  - Cell lines
- METHOD DETAILS
  - Hematology and flow cytometry
  - Zymosan induced peritonitis model
  - Systemic and lung LPS challenge *in vivo*
  - Cell death assays
  - IL-1β release by BMDMs
  - Plasmids and transfection
  - Proteolysis of cell lysates
  - Western Blot
  - Recombinant mouse GSDMD (rGSDMD)
  - Cleavage of rGSDMD and N-terminal sequencing
- QUANTIFICATION AND STATISTICAL ANALYSIS

SUPPLEMENTAL INFORMATION

Supplemental Information can be found online at https://doi.org/10.1016/j.celrep.2019.05.065.

ACKNOWLEDGMENTS

We thank Judy Lieberman, Denis Martinvalet, Michael Murphy, and Jens Stein for reagents. We thank Ruth Lyck for assistance with live-cell imaging. We thank Albert Witt and Urban Deutsch for the RNP microinjection. This work was supported by grants from the Swiss National Science Foundation to C.B. (310030-149790 and 310030-173137) and the Novartis Foundation for medical-biological research.

AUTHOR CONTRIBUTIONS

S.S.B. designed experiments, acquired data, analyzed results, and wrote the manuscript. N.G.F.L. generated mouse Flag-tagged Gsdmd mutants. S.J.S. and G.S.S. produced recombinant mouse Gsdmd and determined cleavage site by sequencing. P.I.B. generated *Sb6a*$^{-/-}$ mice. C.B. conceived the project, designed experiments, analyzed results, supervised the study, and wrote the manuscript. All authors critically reviewed and approved the manuscript.

DECLARATION OF INTERESTS

The authors declare no competing interests.

Received: January 7, 2018
Revised: January 31, 2019
Accepted: May 17, 2019
Published: June 18, 2019

REFERENCES

Adkison, A.M., Raptis, S.Z., Kelley, D.G., and Pham, C.T. (2002). Dipeptidyl peptidase I activates neutrophil-derived serine proteases and regulates the development of acute experimental arthritis. J. Clin. Invest. *109*, 363–371.

Aglietti, R.A., Estevez, A., Gupta, A., Ramirez, M.G., Liu, P.S., Kayagaki, N., Ciferri, C., Dixit, V.M., and Dueber, E.C. (2016). GsdmD p30 elicited by caspase-11 during pyroptosis forms pores in membranes. Proc. Natl. Acad. Sci. USA *113*, 7858–7863.

Aida, T., Chiyo, K., Usami, T., Ishikubo, H., Imahashi, R., Wada, Y., Tanaka, K.F., Sakuma, T., Yamamoto, T., and Tanaka, K. (2015). Cloning-free CRISPR/Cas system facilitates functional cassette knock-in in mice. Genome Biol. *16*, 87.

Akgul, C., Moulding, D.A., and Edwards, S.W. (2001). Molecular control of neutrophil apoptosis. FEBS Lett. *487*, 318–322.

Basilico, P., Cremona, T.P., Oevermann, A., Piersigilli, A., and Benarafa, C. (2016). Increased myeloid cell production and lung bacterial clearance in mice exposed to cigarette smoke. Am. J. Respir. Cell Mol. Biol. *54*, 424–435.

Baumann, M., Pham, C.T., and Benarafa, C. (2013). SerpinB1 is critical for neutrophil survival through cell-autonomous inhibition of cathepsin G. Blood *121*, 3900–3907, S3901–S3906.

Belaaouaj, A., Kim, K.S., and Shapiro, S.D. (2000). Degradation of outer membrane protein A in *Escherichia coli* killing by neutrophil elastase. Science *289*, 1185–1188.

Benarafa, C. (2011). The SerpinB1 knockout mouse a model for studying neutrophil protease regulation in homeostasis and inflammation. Methods Enzymol. *499*, 135–148.

Benarafa, C., and Remold-O'Donnell, E. (2005). The ovalbumin serpins revisited: perspective from the chicken genome of clade B serpin evolution in vertebrates. Proc. Natl. Acad. Sci. USA *102*, 11367–11372.

Benarafa, C., and Simon, H.U. (2017). Role of granule proteases in the life and death of neutrophils. Biochem. Biophys. Res. Commun. *482*, 473–481.

Benarafa, C., Cooley, J., Zeng, W., Bird, P.I., and Remold-O'Donnell, E. (2002). Characterization of four murine homologs of the human ov-serpin monocyte neutrophil elastase inhibitor MNEI (SERPINB1). J. Biol. Chem. *277*, 42028–42033.

Benarafa, C., Priebe, G.P., and Remold-O'Donnell, E. (2007). The neutrophil serine protease inhibitor serpinb1 preserves lung defense functions in Pseudomonas aeruginosa infection. J. Exp. Med. *204*, 1901–1909.

Benarafa, C., LeCuyer, T.E., Baumann, M., Stolley, J.M., Cremona, T.P., and Remold-O'Donnell, E. (2011). SerpinB1 protects the mature neutrophil reserve in the bone marrow. J. Leukoc. Biol. *90*, 21–29.

Bird, C.H., Sutton, V.R., Sun, J., Hirst, C.E., Novak, A., Kumar, S., Trapani, J.A., and Bird, P.I. (1998). Selective regulation of apoptosis: the cytotoxic lymphocyte serpin proteinase inhibitor 9 protects against granzyme B-mediated apoptosis without perturbing the Fas cell death pathway. Mol. Cell. Biol. *18*, 6387–6398.

Bird, C.H., Christensen, M.E., Mangan, M.S., Prakash, M.D., Sedelies, K.A., Smyth, M.J., Harper, I., Waterhouse, N.J., and Bird, P.I. (2014). The granzyme B-Serpinb9 axis controls the fate of lymphocytes after lysosomal stress. Cell Death Differ. *21*, 876–887.

Bliss-Moreau, M., Chen, A.A., D'Cruz, A.A., and Croker, B.A. (2017). A motive for killing: effector functions of regulated lytic cell death. Immunol. Cell Biol. *95*, 146–151.

Cho, Y.S., Challa, S., Moquin, D., Genga, R., Ray, T.D., Guildford, M., and Chan, F.K. (2009). Phosphorylation-driven assembly of the RIP1-RIP3 complex regulates programmed necrosis and virus-induced inflammation. Cell *137*, 1112–1123.

Choi, Y.J., Kim, S., Choi, Y., Nielsen, T.B., Yan, J., Lu, A., Ruan, J., Lee, H.R., Wu, H., Spellberg, B., et al. (2019). SERPINB1-mediated checkpoint of inflammatory caspase activation. Nat. Immunol. *20*, 276–287.

Clancy, D.M., Sullivan, G.P., Moran, H.B.T., Henry, C.M., Reeves, E.P., McElvaney, N.G., Lavelle, E.C., and Martin, S.J. (2018). Extracellular neutrophil proteases are efficient regulators of IL-1, IL-33, and IL-36 cytokine activity but poor effectors of microbial killing. Cell Rep. *22*, 2937–2950.

Cooley, J., Takayama, T.K., Shapiro, S.D., Schechter, N.M., and Remold-O'Donnell, E. (2001). The serpin MNEI inhibits elastase-like and chymotrypsin-like serine proteases through efficient reactions at two active sites. Biochemistry *40*, 15762–15770.

Denault, J.B., and Salvesen, G.S. (2003). Expression, purification, and characterization of caspases. Curr. Protoc. Protein Sci. *Chapter 21*, Unit 21.13.

Ding, J., Wang, K., Liu, W., She, Y., Sun, Q., Shi, J., Sun, H., Wang, D.C., and Shao, F. (2016). Pore-forming activity and structural autoinhibition of the gasdermin family. Nature *535*, 111–116.

Geering, B., and Simon, H.U. (2011). Peculiarities of cell death mechanisms in neutrophils. Cell Death Differ. *18*, 1457–1469.

Gong, D., Farley, K., White, M., Hartshorn, K.L., Benarafa, C., and Remold-O'Donnell, E. (2011). Critical role of serpinB1 in regulating inflammatory responses in pulmonary influenza infection. J. Infect. Dis. *204*, 592–600.

Gonzalez Ramirez, M.L., Poreba, M., Snipas, S.J., Groborz, K., Drag, M., and Salvesen, G.S. (2018). Extensive peptide and natural protein substrate screens reveal that mouse caspase-11 has much narrower substrate specificity than caspase-1. J. Biol. Chem. *293*, 7058–7067.

Hazuda, D.J., Strickler, J., Kueppers, F., Simon, P.L., and Young, P.R. (1990). Processing of precursor interleukin 1 beta and inflammatory disease. J. Biol. Chem. *265*, 6318–6322.

He, S., Wang, L., Miao, L., Wang, T., Du, F., Zhao, L., and Wang, X. (2009). Receptor interacting protein kinase-3 determines cellular necrotic response to TNF-alpha. Cell *137*, 1100–1111.

He, W.T., Wan, H., Hu, L., Chen, P., Wang, X., Huang, Z., Yang, Z.H., Zhong, C.Q., and Han, J. (2015). Gasdermin D is an executor of pyroptosis and required for interleukin-1β secretion. Cell Res. *25*, 1285–1298.

Heid, M.E., Keyel, P.A., Kamga, C., Shiva, S., Watkins, S.C., and Salter, R.D. (2013). Mitochondrial reactive oxygen species induces NLRP3-dependent lysosomal damage and inflammasome activation. J. Immunol. *191*, 5230–5238.

Henry, C.M., Sullivan, G.P., Clancy, D.M., Afonina, I.S., Kulms, D., and Martin, S.J. (2016). Neutrophil-derived proteases escalate inflammation through activation of IL-36 family cytokines. Cell Rep. *14*, 708–722.

Huai, J., Vögtle, F.N., Jöckel, L., Li, Y., Kiefer, T., Ricci, J.E., and Borner, C. (2013). TNFα-induced lysosomal membrane permeability is downstream of MOMP and triggered by caspase-mediated NDUFS1 cleavage and ROS formation. J. Cell Sci. *126*, 4015–4025.

Huang, C.K., Zhan, L., Hannigan, M.O., Ai, Y., and Leto, T.L. (2000). P47(phox)-deficient NADPH oxidase defect in neutrophils of diabetic mouse strains, C57BL/6J-m db/db and db/+. J. Leukoc. Biol. *67*, 210–215.

Jacquemin, G., Margiotta, D., Kasahara, A., Bassoy, E.Y., Walch, M., Thiery, J., Lieberman, J., and Martinvalet, D. (2015). Granzyme B-induced mitochondrial ROS are required for apoptosis. Cell Death Differ. *22*, 862–874.

Jorgensen, I., Rayamajhi, M., and Miao, E.A. (2017). Programmed cell death as a defence against infection. Nat. Rev. Immunol. *17*, 151–164.

Kaiserman, D., and Bird, P.I. (2005). Analysis of vertebrate genomes suggests a new model for clade B serpin evolution. BMC Genomics *6*, 167.

Kambara, H., Liu, F., Zhang, X., Liu, P., Bajrami, B., Teng, Y., Zhao, L., Zhou, S., Yu, H., Zhou, W., et al. (2018). Gasdermin D exerts anti-inflammatory effects by promoting neutrophil death. Cell Rep. *22*, 2924–2936.

Kargi, H.A., Campbell, E.J., and Kuhn, C., 3rd. (1990). Elastase and cathepsin G of human monocytes: heterogeneity and subcellular localization to peroxidase-positive granules. J. Histochem. Cytochem. *38*, 1179–1186.

Kayagaki, N., Warming, S., Lamkanfi, M., Vande Walle, L., Louie, S., Dong, J., Newton, K., Qu, Y., Liu, J., Heldens, S., et al. (2011). Non-canonical inflammasome activation targets caspase-11. Nature *479*, 117–121.

Kayagaki, N., Stowe, I.B., Lee, B.L., O'Rourke, K., Anderson, K., Warming, S., Cuellar, T., Haley, B., Roose-Girma, M., Phung, Q.T., et al. (2015). Caspase-11 cleaves gasdermin D for non-canonical inflammasome signalling. Nature *526*, 666–671.

Kessenbrock, K., Fröhlich, L., Sixt, M., Lämmermann, T., Pfister, H., Bateman, A., Belaaouaj, A., Ring, J., Ollert, M., Fässler, R., and Jenne, D.E. (2008). Proteinase 3 and neutrophil elastase enhance inflammation in mice by inactivating antiinflammatory progranulin. J. Clin. Invest. *118*, 2438–2447.

Kono, H., Orlowski, G.M., Patel, Z., and Rock, K.L. (2012). The IL-1-dependent sterile inflammatory response has a substantial caspase-1-independent component that requires cathepsin C. J. Immunol. *189*, 3734–3740.

Kuida, K., Lippke, J.A., Ku, G., Harding, M.W., Livingston, D.J., Su, M.S., and Flavell, R.A. (1995). Altered cytokine export and apoptosis in mice deficient in interleukin-1 beta converting enzyme. Science *267*, 2000–2003.

Lefrançais, E., Roga, S., Gautier, V., Gonzalez-de-Peredo, A., Monsarrat, B., Girard, J.P., and Cayrol, C. (2012). IL-33 is processed into mature bioactive forms by neutrophil elastase and cathepsin G. Proc. Natl. Acad. Sci. USA *109*, 1673–1678.

Liu, X., and Lieberman, J. (2017). A mechanistic understanding of pyroptosis: the fiery death triggered by invasive infection. Adv. Immunol. *135*, 81–117.

Liu, X., Zhang, Z., Ruan, J., Pan, Y., Magupalli, V.G., Wu, H., and Lieberman, J. (2016). Inflammasome-activated gasdermin D causes pyroptosis by forming membrane pores. Nature *535*, 153–158.

Loison, F., Zhu, H., Karatepe, K., Kasorn, A., Liu, P., Ye, K., Zhou, J., Cao, S., Gong, H., Jenne, D.E., et al. (2014). Proteinase 3-dependent caspase-3 cleavage modulates neutrophil death and inflammation. J. Clin. Invest. *124*, 4445–4458.

Luke, C.J., Pak, S.C., Askew, Y.S., Naviglia, T.L., Askew, D.J., Nobar, S.M., Vetica, A.C., Long, O.S., Watkins, S.C., Stolz, D.B., et al. (2007). An intracellular serpin regulates necrosis by inhibiting the induction and sequelae of lysosomal injury. Cell *130*, 1108–1119.

MacIvor, D.M., Shapiro, S.D., Pham, C.T., Belaaouaj, A., Abraham, S.N., and Ley, T.J. (1999). Normal neutrophil function in cathepsin G-deficient mice. Blood *94*, 4282–4293.

Macleod, T., Doble, R., McGonagle, D., Wasson, C.W., Alase, A., Stacey, M., and Wittmann, M. (2016). Neutrophil elastase-mediated proteolysis activates the anti-inflammatory cytokine IL-36 receptor antagonist. Sci. Rep. *6*, 24880.

Makaryan, V., Zeidler, C., Bolyard, A.A., Skokowa, J., Rodger, E., Kelley, M.L., Boxer, L.A., Bonilla, M.A., Newburger, P.E., Shimamura, A., et al. (2015). The diversity of mutations and clinical outcomes for ELANE-associated neutropenia. Curr. Opin. Hematol. *22*, 3–11.

Martinvalet, D., Dykxhoorn, D.M., Ferrini, R., and Lieberman, J. (2008). Granzyme A cleaves a mitochondrial complex I protein to initiate caspase-independent cell death. Cell *133*, 681–692.

Miao, E.A., Leaf, I.A., Treuting, P.M., Mao, D.P., Dors, M., Sarkar, A., Warren, S.E., Wewers, M.D., and Aderem, A. (2010). Caspase-1-induced pyroptosis is an innate immune effector mechanism against intracellular bacteria. Nat. Immunol. *11*, 1136–1142.

Murphy, J.M., Czabotar, P.E., Hildebrand, J.M., Lucet, I.S., Zhang, J.G., Alvarez-Diaz, S., Lewis, R., Lalaoui, N., Metcalf, D., Webb, A.I., et al. (2013). The pseudokinase MLKL mediates necroptosis via a molecular switch mechanism. Immunity *39*, 443–453.

Oberle, C., Huai, J., Reinheckel, T., Tacke, M., Rassner, M., Ekert, P.G., Buellesbach, J., and Borner, C. (2010). Lysosomal membrane permeabilization and cathepsin release is a Bax/Bak-dependent, amplifying event of apoptosis in fibroblasts and monocytes. Cell Death Differ. *17*, 1167–1178.

Padrines, M., Wolf, M., Walz, A., and Baggiolini, M. (1994). Interleukin-8 processing by neutrophil elastase, cathepsin G and proteinase-3. FEBS Lett. *352*, 231–235.

Perera, N.C., Schilling, O., Kittel, H., Back, W., Kremmer, E., and Jenne, D.E. (2012). NSP4, an elastase-related protease in human neutrophils with arginine specificity. Proc. Natl. Acad. Sci. USA *109*, 6229–6234.

Pop, C., Salvesen, G.S., and Scott, F.L. (2008). Caspase assays: identifying caspase activity and substrates in vitro and in vivo. Methods Enzymol. *446*, 351–367.

Raptis, S.Z., Shapiro, S.D., Simmons, P.M., Cheng, A.M., and Pham, C.T. (2005). Serine protease cathepsin G regulates adhesion-dependent neutrophil effector functions by modulating integrin clustering. Immunity *22*, 679–691.

Ravichandran, K.S. (2011). Beginnings of a good apoptotic meal: the find-me and eat-me signaling pathways. Immunity *35*, 445–455.

Remold-O'Donnell, E., Nixon, J.C., and Rose, R.M. (1989). Elastase inhibitor. Characterization of the human elastase inhibitor molecule associated with monocytes, macrophages, and neutrophils. J. Exp. Med. *169*, 1071–1086.

Scarff, K.L., Ung, K.S., Sun, J., and Bird, P.I. (2003). A retained selection cassette increases reporter gene expression without affecting tissue distribution in SPI3 knockout/GFP knock-in mice. Genesis *36*, 149–157.

Scarff, K.L., Ung, K.S., Nandurkar, H., Crack, P.J., Bird, C.H., and Bird, P.I. (2004). Targeted disruption of SPI3/Serpinb6 does not result in developmental or growth defects, leukocyte dysfunction, or susceptibility to stroke. Mol. Cell. Biol. *24*, 4075–4082.

Scott, F.L., Hirst, C.E., Sun, J., Bird, C.H., Bottomley, S.P., and Bird, P.I. (1999). The intracellular serpin proteinase inhibitor 6 is expressed in monocytes and granulocytes and is a potent inhibitor of the azurophilic granule protease, cathepsin G. Blood *93*, 2089–2097.

Shi, J., Zhao, Y., Wang, K., Shi, X., Wang, Y., Huang, H., Zhuang, Y., Cai, T., Wang, F., and Shao, F. (2015). Cleavage of GSDMD by inflammatory caspases determines pyroptotic cell death. Nature *526*, 660–665.

Taylor, R.C., Cullen, S.P., and Martin, S.J. (2008). Apoptosis: controlled demolition at the cellular level. Nat. Rev. Mol. Cell Biol. *9*, 231–241.

Thiele, D.L., and Lipsky, P.E. (1990). Mechanism of L-leucyl-L-leucine methyl ester-mediated killing of cytotoxic lymphocytes: dependence on a lysosomal thiol protease, dipeptidyl peptidase I, that is enriched in these cells. Proc. Natl. Acad. Sci. USA *87*, 83–87.

Tidwell, T., Wechsler, J., Nayak, R.C., Trump, L., Salipante, S.J., Cheng, J.C., Donadieu, J., Glaubach, T., Corey, S.J., Grimes, H.L., et al. (2014). Neutropenia-associated ELANE mutations disrupting translation initiation produce novel neutrophil elastase isoforms. Blood *123*, 562–569.

Tkalcevic, J., Novelli, M., Phylactides, M., Iredale, J.P., Segal, A.W., and Roes, J. (2000). Impaired immunity and enhanced resistance to endotoxin in the absence of neutrophil elastase and cathepsin G. Immunity *12*, 201–210.

von Gunten, S., Yousefi, S., Seitz, M., Jakob, S.M., Schaffner, T., Seger, R., Takala, J., Villiger, P.M., and Simon, H.U. (2005). Siglec-9 transduces apoptotic and nonapoptotic death signals into neutrophils depending on the proinflammatory cytokine environment. Blood *106*, 1423–1431.

Wallach, D., Kang, T.B., Dillon, C.P., and Green, D.R. (2016). Programmed necrosis in inflammation: toward identification of the effector molecules. Science *352*, aaf2154.

Wang, X., Yousefi, S., and Simon, H.U. (2018). Necroptosis and neutrophil-associated disorders. Cell Death Dis. *9*, 111.

Weinrauch, Y., Drujan, D., Shapiro, S.D., Weiss, J., and Zychlinsky, A. (2002). Neutrophil elastase targets virulence factors of enterobacteria. Nature *417*, 91–94.

Wicki, S., Gurzeler, U., Wei-Lynn Wong, W., Jost, P.J., Bachmann, D., and Kaufmann, T. (2016). Loss of XIAP facilitates switch to TNFα-induced necroptosis in mouse neutrophils. Cell Death Dis. *7*, e2422.

Yanez, A., Coetzee, S.G., Olsson, A., Muench, D.E., Berman, B.P., Hazelett, D.J., Salomonis, N., Grimes, H.L., and Goodridge, H.S. (2017). Granulocyte-monocyte progenitors and monocyte-dendritic cell progenitors independently produce functionally distinct monocytes. Immunity *47*, 890–902.e4.

Zhang, D.W., Shao, J., Lin, J., Zhang, N., Lu, B.J., Lin, S.C., Dong, M.Q., and Han, J. (2009). RIP3, an energy metabolism regulator that switches TNF-induced cell death from apoptosis to necrosis. Science *325*, 332–336.

Zhou, Q., and Salvesen, G.S. (1997). Activation of pro-caspase-7 by serine proteases includes a non-canonical specificity. Biochem. J. *324*, 361–364.

STAR★METHODS

KEY RESOURCES TABLE

REAGENT or RESOURCE	SOURCE	IDENTIFIER
Antibodies		
anti-mouse Ly-6G APC/Cy7	Biolegend	Clone 1A8, Cat.#127624; RRID: AB_10640819
anti-mouse CD115 (CSF-1R) PE	Biolegend	Clone AFS98, Cat.#135506; RRID: AB_1937253
anti-mouse/human CD11b PE/Cy7	Biolegend	Clone M1/70, Cat.#101216; RRID: AB_312799
anti-mouse CD11c APC	Biolegend	Clone N418, Cat.#117310; RRID: AB_313779
anti-mouse CD45R (B220) Pacific Blue	Biolegend	Clone RA3-6B2, Cat.#103227; RRID: AB_492876
anti-mouse Ly6C Pacific Blue	Biolegend	Clone HK1.4, Cat.#128014; RRID: AB_1732079
anti-mouse CD3 PE/Cy7	Biolegend	Clone 17A2, Cat.#100220; RRID: AB_1732057
anti-mouse CD4 APC	Biolegend	Clone GK1.5, Cat.#100412; RRID: AB_312697
anti-mouse CD8a APC/Cy7	Biolegend	Clone 53-6.7, Cat.#100714; RRID: AB_522312
anti-mouse NK1.1 APC	Biolegend	Clone PK136, Cat.#108710; RRID: AB_313397
Anti-mouse CD16/CD32 purified	Biolegend	Clone 2.4G2, Cat.#101302; RRID: AB_312801
anti-mouse Siglec F PE	BD Bioscience	Clone E50-2440, Cat.#562068; RRID: AB_10896143
anti-mouse CD45 V500	BD Bioscience	Clone 30-F11, Cat.#561487; RRID: AB_10697046
Mouse Anti-mouse NDUFS3	Invitrogen	Cat.#459130; RRID: AB_2532226
Mouse Anti-mouse NDUFS1	Santa Cruz	Clone E-8, Cat.#sc-271510; RRID: AB_10655669
Rabbit anti-mouse Actin	Abcam	Cat.#ab8227; RRID: AB_2305186
Rabbit anti-human GSDMD	Sigma	Cat.#G7422; RRID: AB_1850381
Rabbit anti-mouse GSDMD	Novus	Cat.#NBP2-33244
Mouse anti-Flag M2	Sigma	Cat.#F1804; RRID: AB_262044
Chemicals, Peptides, and Recombinant Proteins		
Annexin V APC	Biolegend	Cat.#640941
7-AAD	Biolegend	Cat.#420404
L-leucyl-L-leucine methyl ester	Bachem	Cat.#G-2550
Q-VD-OPh hydrate	ApexBio	Cat.#A1901
Necrostatin-1	Enzo Life Science	Cat.#BML-AP309-0100
Mouse TNF-α	Promokine	Cat.#D-63720
Actinomycin D	Promokine	Cat.#PK-CA577-1036-5MG
MitoQ	In house	Provided by Michael Murphy
Recombinant caspase-11	Enzo Life Science	Cat.#BML-SE155-5000
Purified human Cathepsin G	Athens Research Technologies	Cat.#16-14-030107
Purified human Elastase	Athens Research Technologies	Cat.#16-14-051200
Purified human Proteinase-3	Athens Research Technologies	Cat.#16-14-161820
Cathepsin G Inhibitor	Calbiochem	Cat.#429676-93-7
Suc-AAPF-AMC	Bachem	Cat. #4012873.0050
Immobilon-P membrane	Millipore	
Zymosan A from *S. cerevisiae*	Sigma	Cat.#ZA250
LPS from *P. aeuroginosa*	Sigma	Cat.#L8643
Mouse recombinant M-CSF	PeproTech	Cat.#315-02
Ultra Pure LPS from *E. coli*	InvivoGen	Cat.#tlrl-3pelps
Nigericin	InvivoGen	Cat.#tlrl-nig
ATP	InvivoGen	Cat.#tlrl-atpl
Alt-R™ S.p. Cas9 Nuclease 3NLS	Integrated DNA Technologies (IDT)	Lot.#289717
Alt-R™ CRISPR tracrRNA	Integrated DNA Technologies (IDT)	Lot.#275957

(*Continued on next page*)

Continued		
REAGENT or RESOURCE	SOURCE	IDENTIFIER
Nuclease Free Duplex Buffer	Integrated DNA Technologies (IDT)	Lot.#271987
Restore™ Western Blot Stripping Buffer	ThermoFisher Scientific	Cat. #21059
TurboFect Transfection Reagent	ThermoFisher Scientific	Cat. #R0531
Commercial Assays		
pFlag-CM-4 mouse GSDMD plasmid	Addgene; Liu et al., 2016	Cat.#80950; RRID: Addgene_80950
pcDNA3.1 human GSDMD plasmid	GenScript, this paper	N/A
pET29b(+)	Novagen (Sigma)	Cat.#71463-M
Mouse IL-1β ELISA	Thermo Fisher Scientific (eBioscience)	Cat.#88-7013-88; RRID: AB_2574946
Mouse IL-6 ELISA	Thermo Fisher Scientific (eBioscience)	Cat.#88-7064-88; RRID: AB_2574990
Mouse TNF-α ELISA	Thermo Fisher Scientific (eBioscience)	Cat.#88-7324-88; RRID: AB_2575080
Differential Quik Stain Kit (modified Giemsa)	Electron Microscopy Science	Cat.#26096-50
Experimental Models: Cell Lines		
Human monocyte THP-1	ATCC	Cat.#ATCC TIB-202, gift from Alfred Walz
Human embryonic kidney HEK293	ATCC	Cat.#ATCC CRL-1573
Experimental Models: Organisms/Strains		
Serpinb1a$^{tm1.1Cben}$	Benarafa et al., 2007	RRID: MGI: 5707644
Serpinb6a$^{tm1.1Pib}$	Scarff et al., 2003	RRID: MGI: 3720026
Sb1a.Sb6a$^{-/-}$	In house	N/A
Ctsg^{tm1Ley}	MacIvor et al., 1999	RRID: MGI: 3526662
CatG.Sb1a.Sb6a$^{-/-}$	In house	N/A
B6(Cg)-*Ncf1*^{m1J}/J	JAX Labs; Huang et al., 2000	Cat.# 004742; RRID: IMSR_JAX: 004742
B6J.129-*Casp1*^{tm1Flv}	Kuida et al., 1995	RRID: MGI: 3711186
Gsdmd$^{em1, em4, em5, em6}$	In house	N/A
Gsdmd $^{em1, em4, em5, em6}$.*Sb1a.Sb6a*$^{-/-}$	In house	N/A
Software and Algorithms		
Prism 8 (version 8.0)	GraphPad Software	https://www.graphpad.com/scientific-software/prism/
Image Studio 4.0	LI-COR	https://www.licor.com/bio/image-studio/
Imaris Software	Oxford Instruments	https://imaris.oxinst.com/

CONTACT FOR REAGENT AND RESOURCE SHARING

Further information and requests for resources and reagents should be directed to and will be fulfilled by the Lead Contact, Charaf Benarafa (charaf.benarafa@vetsuisse.unibe.ch).

EXPERIMENTAL MODEL AND SUBJECT DETAILS

Mouse husbandry

All animal studies were approved by the Cantonal Veterinary Office of Bern and conducted in accordance with the Swiss federal legislation on animal welfare. Mice were kept in SPF facilities, in individually ventilated cages (Tecniplast, blue line), with 12/12 light/dark cycle, autoclaved acidified water, autoclaved cages including food, bedding and environmental enrichment. Age and gender of mice is indicated for each *in vivo* or *ex vivo* model described below as well as in figure legends.

Previously described mouse lines

All mice were in C57BL/6J background or backcrossed for at least 10 generations. *Sb1a*$^{-/-}$ (*Serpinb1a*$^{tm1.1Cben}$) and *Sb6a*$^{-/-}$ (*Serpinb6a*$^{tm1.1Pib}$) mice were generated previously (Benarafa et al., 2007; Scarff et al., 2003). *CatG*$^{-/-}$ (*Ctsg*^{tm1Ley}) mice were provided by Christine Pham (Washington University, St. Louis) (MacIvor et al., 1999), *Ncf1*$^{-/-}$ (*Ncf1*^{m1J}) mice were from The Jackson Laboratory (Huang et al., 2000). *Casp1/11*$^{-/-}$ (B6J.129-*Casp1*^{tm1Flv}) mice (Kuida et al., 1995) were provided by Jens Stein. We confirmed by PCR and sequencing that the *Casp1/11*$^{-/-}$ mice (but not any other strain) carried the *Casp*^{129} 5-nt deletion in *Casp11* described previously (Kayagaki et al., 2011).

Newly generated mouse lines

Sb1a.Sb6a$^{-/-}$ mice were generated by mating compound heterozygous F1 mice. The two genes are separated by 1.2 Mb (0.25cM) on mouse chromosome 13 and we observed 5 crossover events from 378 F2 pups, of which only one crossover event had two deleted alleles on the same chromosome (*Sb1a*$^{+/-}$.*Sb6a*$^{-/-}$) and the others had two wild-type alleles on the same chromosome (*Sb1a*$^{+/-}$.*Sb6a*$^{+/+}$ or *Sb1a*$^{+/-}$.*Sb6a*$^{+/+}$). *Gsdmd*$^{-/-}$ mice were generated at the transgenic unit of the Theodor Kocher Institute, University of Bern by microinjection of wild-type and *Sb1a.Sb6a*$^{-/-}$ zygotes with ribonucleoprotein (RNP) complexes as described (Aida et al., 2015) and detailed hereafter. Recombinant Cas9 nuclease, tracrRNA, crRNA and nuclease-free duplex buffer were from IDT. Target-specific crRNA sequence used was AGCATCCTGGCATTCCGAG, which was previously shown to successfully target *Gsdmd* in mouse zygotes (Shi et al., 2015). To prepare RNPs, tracrRNA and crRNA stock solutions were reconstituted at 10 μM concentrations in nuclease-free duplex buffer and stored at-20°C. tracrRNA and crRNA were mixed (4.5μl each) and incubated at 95°C for 2 minutes, then cooled down at room temperature for at least 15 minutes for annealing of the duplex. EmbryoMax buffer (Millipore) (20.5μl) was added to the RNA duplex at room temperature, mixed by pipetting twice. Cas9 protein (0.5μl) was added to the RNA duplex and mixed again by pipetting. The RNP was incubated at 37°C for 20 minutes, centrifuged at 18'000 g for 10 min at 4°C and placed on ice until microinjection into the male pronucleus of zygotes on the same day. After overnight incubation at 37°C, live 2-cell stage embryos were transferred into the infundibulum of pseudopregnant CD1 females using standard protocols. Founders were positively screened by PCR and T7 endonuclease assay. Mosaic founders were crossed with C57BL/6J or *Sb1a.Sb6a*$^{-/-}$ and mutated alleles in F1 mice were identified by DNA sequencing (Figure S7). F1 mice with identical mutations were intercrossed to generate *Gsdmd*$^{-/-}$, *Gsdmd.Sb1a.Sb6a*$^{-/-}$ mice. F2 progeny of four distinct *Gsdmd*$^{-/-}$ mouse lines and their littermates were studied.

Mouse cohorts

For each experimental set up involving *in vivo* experimentation or isolated cells, gender and age of the mice is indicated in METHODS DETAILS below and in figure legends. For *in vivo* experiments and determination of leukocyte numbers in blood and bone marrow, animals were used at 6 weeks of age and data was pooled and analyzed using mice from both sex, except for the model of lung instillation of LPS, where only females were used as indicated below. For assays using isolated primary mouse leukocytes, mice were used between 6-12 weeks of age. Data was pooled from both male and female mice from all genotypes. Figure legends indicate the numbers of individual mice per genotype (n) and explicitly mention the number of independent experiments that we have performed.

Cell lines

Human embryonic kidney (HEK293) cells were cultured in DMEM supplemented with 10% heat-inactivated FBS and 1% penicillin/streptomycin and maintained at 37°C in 5% CO_2. Human monocytic cell line THP-1 cells were cultured in RPMI supplemented with 10% heat-inactivated FBS and 1% penicillin/streptomycin and maintained at 37°C in 5% CO_2. In cell death assays, primary mouse bone marrow leukocytes were cultured in DMEM supplemented with 1% FBS and 1% penicillin/streptomycin at 1x10^6 cells/ml. Primary mouse bone marrow-derived macrophages (BMDMs) were generated by culturing bone marrow leukocytes in RPMI supplemented with 10% FBS, 1% penicillin/streptomycin and 10ng/ml M-CSF (PeproTech) for 7 days. Each preparation of primary cell cultures were from 1-2 sex- and age-matched 6-12 week-old male and female mice of each genotype.

METHOD DETAILS

Hematology and flow cytometry

Erythrocyte (RBC), platelet (PLT) and total white blood cell (WBC) counts were determined in whole blood collected in EDTA of 6 week-old female and male mice using a VetABC hematology analyzer. Blood and bone marrow leukocyte subsets percentages and cell death kinetics of bone marrow cells were determined using a 4-color FACS Calibur (BD Biosciences) using single cell suspensions blocked with anti-CD16/CD32 (clone 2.4G2) and stained for 30-40 min on ice with fluorescently labeled antibodies (1:200; BioLegend, BD Biosciences) as previously (Benarafa et al., 2011). Analysis was performed using FlowJo gating within nucleated live CD45$^+$ cells as neutrophils (CD11b$^+$/Ly6G$^+$), monocytes (CD11b$^+$/CD115$^+$), B cells (CD45R/B220$^+$), eosinophils (SSC^{high}/SiglecF$^+$), NK cells (NK1.1$^+$/CD3^{neg}) and T cells (CD3$^+$). Apoptosis and necrosis of neutrophils and monocytes *in vitro* was determined by Annexin V-allophycocyanin and 7-aminoactinomycin D (7AAD) labeling for 15min at room temperature prior to FACS analysis. Flow cytometry sorting of neutrophils (CD11b$^+$/Ly6G$^+$) was performed on single-cell suspensions of bone marrow leukocytes using a FACS Aria II sorter (BD Biosciences) at the flow cytometry core facility of the University of Bern.

Zymosan induced peritonitis model

Groups of 2-3 female or male 6 week-old mice per genotype were injected intraperitoneally with 0.5mg opsonized zymosan (1mg/ml). The experiment was repeated 4 times. Peritoneal cells were collected with 5ml PBS supplemented with 1% FBS 4 hours after injection. Cells were counted manually in a Neubauer chamber. Relative percentages of live leukocyte subsets were determined by flow cytometry, analysis was performed using FlowJo gating within nucleated live CD45$^+$ cells as neutrophils (CD11b$^+$/Ly6G$^+$) and macrophages (CD11b$^+$/CD115$^+$). Phagocytosis of zymosan particles was determined by microscopy analysis of cytospins (Shandon)

stained with Differential Quik stain (Electron Microscopy Science). One hundred cells/mouse were counted to calculate the percentage of zymosan positive cells and 40 zymosan positive neutrophils/mouse were further evaluated for the number of particles per phagocyte.

Systemic and lung LPS challenge *in vivo*

Systemic inflammation was induced in groups of male and female mice by intraperitoneal injection of 10μg/g LPS from *P. aeruginosa* (Sigma, L8643) diluted in 0.9% NaCl. EDTA plasma was collected 2 or 6 hours after injection. Local lung inflammation was induced in groups of anesthetized female mice (intraperitoneal ketamine/xylazine 100mg/kg, 10mg/kg, respectively) by intranasal instillation of LPS (10μg/mouse in 20μl). Bronchoalveolar lavage (BAL) was collected with 3x 1ml PBS supplemented with 1% FBS 14 hours after injection. TNF-α, IL-6 and IL-1β in plasma and BAL were measured by ELISA (eBioscience).

Cell death assays

In cell death induction assays, leukocytes (1x10^6 cells/ml) were incubated at indicated concentrations with L-leucyl-L-leucine methyl ester (LLME) (G-2550; Bachem), Q-VD-OPh (ApexBio), necrostatin-1 (Enzo LifeScience), TNF-α (Promokine) and actinomycin (PeproTech). MitoQ was a gift from Michael Murphy. Viability was assessed by flow cytometry as described above. Live cell images were acquired on a Zeiss Axio Observer of total bone marrow cells of female and male 6-12 week-old mice stained for 30-40 min on ice with fluorescently labeled antibody for neutrophils ($Ly6G^+$) and DAPI to visualize dead cells. Cells were kept at 37°C following administration of 100 μM LLME. Life cell images were taken every 30sec over a time frame of 120min. Live cell images over time were analyzed using dot quantification feature of IMARIS quantifying the number of $Ly\text{-}6G^+$ neutrophils and $DAPI^+$ dead cells over time.

IL-1β release by BMDMs

BMDMs (2x10^6 cells/ml) were primed with 100ng/ml ultra-pure LPS (InvivoGen) for 5 hours followed by stimulation with 5mM ATP or 5 μM nigericin (InvivoGen) for 3 and 18 hours in RPMI supplemented with 10% FBS, 1% penicillin/streptomycin and 10ng/ml M-CSF (PeproTech). Mature IL-1β in culture medium was measured by ELISA (eBioscience).

Plasmids and transfection

pFlag-CMV-4 containing N-terminal Flag-tagged mouse GSDMD was a gift from Judy Lieberman (Addgene plasmid # 80950) (Liu et al., 2016). Human GSDMD cDNA was synthetized and cloned into pcDNA3.1(+)-N-DYK (Flag) using BamHI/EcoRI (GenScript). Alanine substitution mutants were generated using Q5 site-directed mutagenesis kit (NEB). WT and mutant Flag-GSDMD plasmids were purified (Macherey-Nagel) and verified by DNA sequencing (Microsynth). Transient transfection of HEK cells with Flag-Gsdmd plasmids was performed using TurboFect (ThermoFisher Scientific) following the manufacturer's procedure. In brief, 2x10^5 HEK cells were seeded in a 6-well plate followed by transfection with 6 μL TurboFect and 4 μg plasmid DNA. HEK cells were grown without selection pressure until 90% confluency after transfection to allow high protein yield during lysis.

Proteolysis of cell lysates

HEK and THP-1 cells were lysed in 0.1% Triton X-100 lysis buffer without protease inhibitors followed by 2x 30sec sonication (Soniprep 150 plus, MSE). Lysates were clarified at 10'000 g for 10min at 4°C and supernatant was collected. Total protein concentration in lysates was determined by the BCA assay (ThermoFisher Scientific). Cell lysates (12.5 μg HEK; 25μg THP-1) were incubated for 1h at 37°C with recombinant caspase-11 (175nM final concentration) (Enzo LifeScience, BML-SE155-5000) or with purified human CatG, NE or PR3 (Athens Research Technologies) at indicated concentrations ranging from 4-136nM. Where indicated, Q-VD-OPh (1mM)(ApexBio) or cathepsin G inhibitor I (CatG-Inh)(1mM)(Calbiochem, 429676-93-7) were preincubated for 5 min at 37°C before the protease treatment. Proteolysis was stopped by adding final concentration of 1x Laemmli Buffer with DTT (25mM) to the reaction and incubated for 5 min at 95°C prior to loading on SDS-PAGE.

Western Blot

Lysates were resolved by SDS-PAGE under reducing conditions using Tris-Glycine buffer. After transfer on nitrocellulose, blocking was performed using 0.5% skimmed milk and blots were probed with anti-Flag M2 (Sigma, F1804), rabbit anti-GSDMD (Sigma, G74222 antibodies. Blots were stripped (Restore Western Blot Stripping Buffer, ThermoFisher, 21059) and reprobed with anti-β-actin antibody (Abcam, ab8227). Cleavage of NDUFS3 and NDUFS1 was performed on sorted bone marrow neutrophils, which were pre-incubated in PBS with protease inhibitor cocktail (Roche) for 5 min at 37°C before lysis in 1% NP-40 lysis buffer. Blots were probed with monoclonal mouse anti-NDUFS1 (Santa Cruz, E-8, sc-271510) and monoclonal mouse-anti NDUFS3 (Invitrogen, 459130) antibodies, both gifts from Denis Martinvalet.

Recombinant mouse GSDMD (rGSDMD)

The sequence encoding mouse full length GSDMD was purchased from Integrated DNA Technologies and cloned into pET29b(+) (Novagen) containing a C-terminal His tag and transformed into BL21 (DE3) competent *E. coli*. Expression was induced with 0.2mM isopropyl β-D-1-thiogalactopyranoside (IPTG) for 4 hours at 25°C shaking at 250 RPM. The GSDMD cell pellets were

resuspended in 50mM HEPES, 100 mM NaCl, pH 8.0 and lysed via sonication. Cell lysates were centrifuged at 4°C for 30 minutes at 29,000 x g, supernatants were filtered through a 0.22μm filter (Millipore) and the soluble fractions were applied to a 1ml Ni-chelating Sepharose resin (GE Healthcare Life Sciences) in a chromatography column. The rGSDMD-bound resin was washed in 50mM HEPES, 500mM NaCl, pH 8.0 and then eluted in 50mM HEPES, 100mM NaCl, pH 8.0 with stepwise increments of imidazole from 12.5 – 100 mM. rGSDMD purity was analyzed by 4%–12% Bis-Tris SDS/PAGE gel (Novex Life Technologies) stained with Instant Blue (Expedeon).

Cleavage of rGSDMD and N-terminal sequencing

To determine the active concentration of CatG (Athens Research Technologies), a serial dilution series of Ac-AAPF-OPh_2 was incubated with CatG for 30 minutes at 37°C. The fluorogenic substrate Suc-AAPF-AMC was added to a final concentration of 100μM in 100μl of assay buffer (100mM Tris-HCL pH 7.5 500mM NaCl) and enzymatic activity was measured. Velocities were plotted against inhibitor concentration allowing the calculation of active enzyme concentration (Denault and Salvesen, 2003). Active site titrated CatG was subjected to two-fold series dilutions and incubated separately for 30 minutes at 37°C with 2μM of GSDMD in 100mM Tris-HCL pH 7.5 500mM NaCl in a final assay volume of 20μl. Reactions were terminated by heating at 95°C with 10μl of 3x SDS loading buffer to give a final concentration of 1x loading buffer. Samples were analyzed on 4%–12% Bis-Tris SDS-PAGE gels by Instant Blue staining. The gels were then scanned and imported to Image Studio (LI-COR Biosciences) for protein band intensity quantification. Band intensity values were plotted against enzyme concentration and IC_{50} values were determined via GraphPad Prism. Those values were then used to determine k_{cat}/K_M using the following equation $k_{cat}/K_M = ln2/(E_{1/2} * t)$. Here, k_{cat}/K_M is the second order rate constant for substrate hydrolysis, $E_{1/2}$ is the concentration of protease for which half the substrate is consumed, E is the concentration of enzyme, and t is the incubation time (Pop et al., 2008). Protein sample was resolved by SDS/PAGE and transferred to an Immobilon-P membrane (Millipore, Bedford, MA, USA) by electroblotting. The membrane was briefly stained with Coomassie Brilliant Blue R-250, destained and washed with water. The appropriate band was excised and sequenced by Edman degradation with a ABI Procise at UC Davis Proteomics Core Facility.

QUANTIFICATION AND STATISTICAL ANALYSIS

Statistical analysis and graphs were generated using Prism 8.0 (GraphPad, San Diego, CA). As indicated in figure legends, independent experiments were performed and data was pooled. Where applicable data was shown for each replicate or mouse using scatterplots and horizontal lines or bars showed mean ± SEM. Box and whiskers showed median, interquartile range, 5–95 percentiles and individual values above 95th percentile. For analysis, non-parametric tests were used to analyze data from *in vivo* and *ex vivo* studies. Experiments were analyzed by Mann-Whitney test, one-way or two-way ANOVA with Tukey post-test as appropriate and as indicated in figure legends. $p < 0.05$ was considered statistically significant (****$p < 0.0001$; ***$p < 0.001$; **$p < 0.01$; *$p < 0.05$).